***In vitro* binding assay.** To analyze the interaction of GST-ORF44 with ORF49, GST-ORF44, GST-ORF44F129A, or GST-ORF44P recombinant protein was expressed in and purified using BugBuster master mix (Merck Millipore, Darmstadt, Germany) from *E. coli* BL21 transformed with pGEX/ORF44, pGEX/ORF44F129A, or pGEX/ORF44P as described above. ORF49p was expressed in MeWo cells by transfection of CAG/ORF49 using Lipofectamine 2000 and solubilized as described above. GST-ORF44 recombinant protein was bound to glutathione Sepharose 4B (GE Healthcare Bio-Sciences) overnight at 4°C, washed with PBS three times, pelleted, and reacted with soluble ORF49p overnight at 4°C. The bead–GST-ORF44 recombinant protein–ORF49p complex was washed with RIPA lysis buffer three times, pelleted, suspended in SDS-PAGE sample buffer, boiled, and subjected to SDS-PAGE and immunoblotting as described above.

Protein identification by MS. MeWo cells were infected with pOka by cell-to-cell infection and lysed with RIPA lysis buffer as described above. The cell lysates from pOka- or mock-infected MeWo cells were precleared with protein G Sepharose and subjected to immunoprecipitation with anti-ORF49 Ab cross-linked protein G Sepharose. The immunoprecipitates were separated by SDS-PAGE and stained with a SilverQuest silver staining kit (Invitrogen). Protein bands were excised from the gel and digested with trypsin (sequencing grade; Promega, Madison, WI) according to published procedures (38). Nano-liquid chromatography-tandem mass spectrometry (nano-LC-MS/MS) analyses were performed on an LTQ-Orbitrap XL mass spectrometer (Thermo Fisher Scientific, Waltham, MA) equipped with a nano-electrospray ionization (nano-ESI) source (AMR, Tokyo, Japan) and coupled to a Paradigm MG4 pump (Michrom Bioresources, Auburn, CA) and autosampler (HTC PAL; CTC Analytics, Zwingen, Switzerland). A spray voltage of 1,800 V was applied. The peptide mixture was separated on a Magic C_{18} AQ column (100 μm by 150 mm, 3.0-μm particle size, 300 Å; Michrom Bioresources) with a flow rate of 500 nl/min. The linear gradient was as follows: 5% to 45% B in 30 min, 45% to 95% B in 0.1 min, 95% B for 2 min, and finally 5% B (solvent A = 0.1% formic acid in 2% acetonitrile, and B = 0.1% formic acid in 90% acetonitrile). Intact peptides were detected in the Orbitrap at a resolution of 60,000. For the LC-MS/MS analysis, six precursor ions were selected for subsequent MS/MS scans in a data-dependent acquisition mode following each full scan (*m/z*, 350 to 1,500). A lock mass function was used for the LTQ-Orbitrap to obtain constant mass accuracy during the gradient analysis. Peptides and proteins were identified by automated database searches using Proteome Discoverer v.1.1 (Thermo Fisher Scientific, Waltham, MA) against human entries or all entries of the Swiss-Prot protein database (version 3.26) with a precursor mass tolerance of 10 parts per million (ppm), a fragment ion mass tolerance of 0.8 Da, and strict trypsin specificity, allowing for up to two missed cleavages. Cysteine carbamidomethylation was set as a fixed modification, and methionine oxidation was allowed as a variable modification.

Plaque size and infectious-center assays for growth kinetics. To analyze the growth kinetics of the recombinant viruses, infectious-center assays were performed as described previously (6) with slight modifications. Briefly, 5×10^5 MeWo or MeWoORF49 cells were seeded on one well of a 12-well plate and inoculated with 50 PFU of cell-free virus per well. For the plaque size measurement, the infected cells were cultured for 7 days. For the infectious-center assay, infected cells were harvested at 24-h intervals and then titrated on newly prepared cells. The cells were fixed in 30% methanol and 70% acetone and stained with an anti-gE MAb (clone 9) and secondary ECL anti-mouse IgG horseradish peroxidase-linked whole antibody (GE Healthcare Bio-Sciences). The stain was developed with 3,3′,5,5′-tetramethylbenzidine-H (TMB-H) peroxidase substrate (Moss, Inc., Pasadena, MD). Images of the plaques were captured and traced, and the number of plaques was counted, or the plaque area was measured using ImageJ (http://rsbweb.nih.gov/ij/).

RESULTS

ORF49 functions in the efficient production of infectious progeny virus. To examine the mechanism of action of ORF49, we performed loss-of-function and gain-of-function analyses by generating an ORF49-defective virus, rpOkaORF49M1L, and its revertant virus, rpOkaORF49M1LRev, from the pOka-BACORF49M1L and pOka-BACORF49M1LRev genomes, respectively (Fig. 1A and C). In addition, the MeWoORF49 cell line was established to express ORF49 constitutively in MeWo cells in which the previous ORF49-defective virus, rpOkaΔ49, specifically showed an impaired growth phenotype (6), and gain-of-function analysis was performed by ORF49 *trans*-complementation assay.

None of the assayed viral proteins, including glycoprotein H (gH), ORF61 protein (ORF61p), ORF44p, and ORF49p, were detected in MeWo cells (Fig. 2A, lane 1). In MeWoORF49 cells, ORF49p was the only protein detected among the tested viral proteins (Fig. 2A, lane 2), and its expression level was comparable to that of ORF49p in rpOka-infected MeWo cells (Fig. 2A, lane 3). In rpOkaORF49M1L-infected cells, ORF49p was not detected in the infected MeWo cells (Fig. 2A, lane 4) or in the viral particles (Fig. 2C, lane 2), although gH and ORF61p were clearly expressed in infected cells (Fig. 2A, lane 4), as was gH in the viral particles (Fig. 2C, lane 2). The rpOkaORF49M1LRev line expressed all of the viral proteins tested (Fig. 2A, lane 5), similar to rpOka-infected MeWo cells (Fig. 2A, lane 3).

To confirm the ORF49-defective phenotype and perform gain-of function analysis, plaque formation was analyzed on MeWo and MeWoORF49 cells (Fig. 3A). Plaque sizes were similar between rpOka-infected MeWo and MeWoORF49 cells (Fig. 3A, lanes 1 and 2), indicating that the exogenous expression of ORF49 had neither positive nor negative effects on normal VZV infection. Similar to our previous results using rpOkaΔ49, rpOkaORF49M1L formed significantly smaller plaques on MeWo cells (Fig. 3A, lane 3) than on MeWoORF49 cells, and this reduction was recovered in the revertant virus infection in MeWo cells (Fig. 3A, lane 5) and completely rescued by the exogenous expression of ORF49 in MeWoORF49 cells (Fig. 3A, lane 4). Consistent with the plaque formation assay results, rpOkaORF49M1L propagated on MeWo cells showed slower growth than rpOka or rpOkaORF49M1LRev on MeWo or MeWoORF49 cells in an infectious-center assay, and the growth impairment of rpOkaORF49M1L was completely rescued by exogenous ORF49p in MeWoORF49 cells (Fig. 3B).

During the preparation of cell-free viruses, another strikingly different phenotype of the ORF49 defect was observed. As summarized in Table 2, the titer of cell-free virus or plaque size formed by the cell-free virus infection of rpOka was almost the same whether the virus was propagated on MeWo or MeWoORF49 cells or titrated on MeWo or MeWoORF49 cells, again indicating that the exogenous ORF49p had no effect on normal VZV infection. When rpOkaORF49M1L was propagated on MeWo cells, the titer of cell-free virus was 3 to 5% of that observed with propagation of MeWoORF49 cells, and the plaque size depended on the kind of cells used for titration but not on the kind used for propagation. In addition, the rpOkaORF49M1L particles isolated from MeWoORF49 cells contained abundant ORF49p (Fig. 2C, lane 3) and produced almost the same titer of cell-free virus as the parental virus but formed significantly smaller plaques on MeWo cells (Table 2). This gain-of-function analysis performed using the ORF49 *trans*-complementation system suggested that the incom-

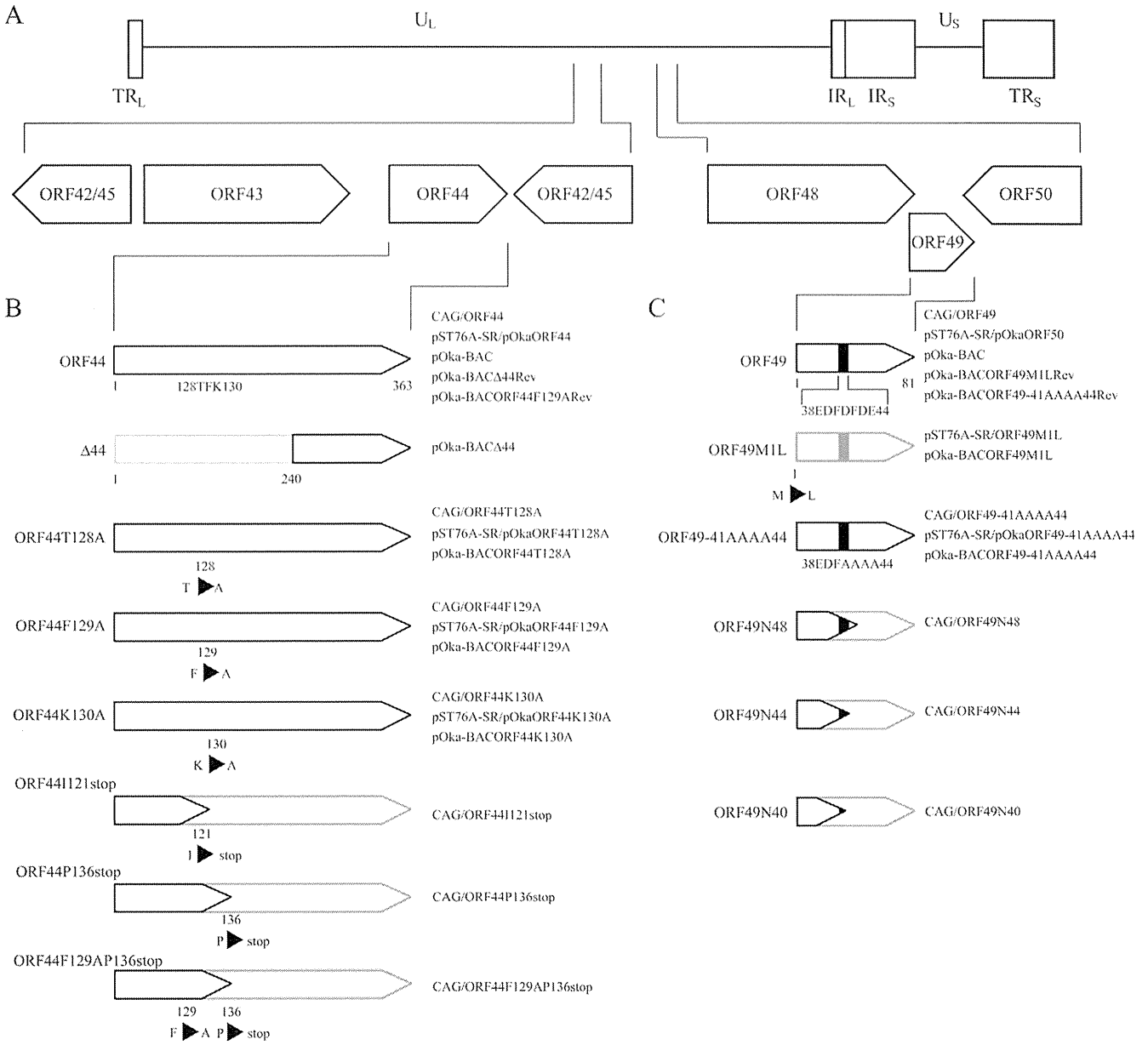

FIG 1 Schematics showing the plasmids and recombinant BAC genomes for ORF44 and ORF49. (A) Location of the ORF44 and ORF49 genes in the unique long region (U_L) segment of the genome of VZV strain pOka; terminal repeats (TR), unique short region (U_S), and internal repeats (IR) are indicated. (B) The wild type, deleted Δ44 region, and amino acid substitutions in ORF44p are shown. (C) The wild type, amino acid substitutions at the first methionine or the carboxyl-terminal half of the acidic cluster from amino acid positions 41 to 44, and the carboxyl-terminal truncations within ORF49p are shown. The acidic cluster is indicated as a black box. (B and C) Unexpressed regions of the mutant proteins are shown in gray outlined shapes. The names of relevant BACs, shuttle plasmids, and mammalian expression plasmids containing mutations are shown on the right.

ing ORF49p from the viral particles into the cells was not functional in any step and revealed that *de novo* ORF49p functioned in the production of infectious progeny viruses required for efficient propagation.

Furthermore, to examine the role of ORF49 in the production of infectious progeny viruses in detail, we redesigned our study on ORF49 to investigate its function by analyzing its binding partners.

Identification of the ORF44 protein as the binding partner for ORF49. ORF49p was immunoprecipitated from pOka- or mock-infected MeWo cells using an anti-ORF49 antibody (Ab), and the coimmunoprecipitating proteins were separated in a denaturing gel and visualized by silver staining (Fig. 4A). An approximately 36-kDa band was coimmunoprecipitated with the 13-kDa band corresponding to the ORF49p in pOka-infected MeWo cell lysates (Fig. 4A, lane 1). This 36-kDa band was identified as the ORF44 protein (ORF44p) of VZV by LC-MS/MS analysis (24.3% coverage of 363 amino acids).

ORF44p was specifically detected as a 36-kDa band in all recombinant VZV-infected MeWo cells, including rpOkaORF49M1L, by

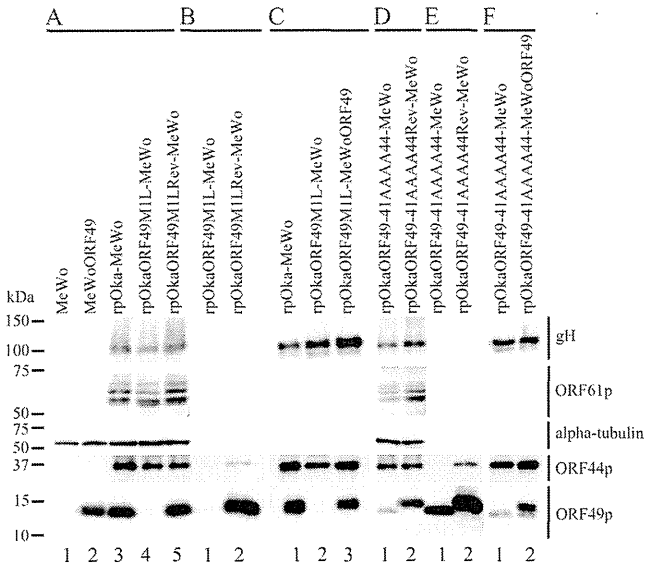

FIG 2 Expression and interaction of viral proteins during ORF49 mutant virus infection. (A) Proteins expressed in mock-infected MeWo cells (lane 1), mock-infected MeWoORF49 cells (lane 2), rpOka-infected MeWo cells (lane 3), rpOkaORF49M1L-infected MeWo cells (lane 4), and rpOkaORF49M1LRev-infected MeWo cells (lane 5) were visualized with Abs against gH, ORF61p, α-tubulin, ORF44p, and ORF49p. (B) The interaction between ORF44p and ORF49p was analyzed in rpOkaORF49M1L-infected cells (lane 1) and rpOkaORF49M1LRev-infected cells (lane 2). Immunoprecipitates obtained with an anti-ORF49 Ab from each type of virus-infected cells were electrophoretically separated and visualized using anti-ORF44 and anti-ORF49 Abs. (C) The viral proteins incorporated into virions from rpOka-infected MeWo cells (lane 1), rpOkaORF49M1L-infected MeWo cells (lane 2), and rpOkaORF49M1L-infected MeWoORF49 cells (lane 3) were visualized using Abs against gH, ORF61p, ORF44p, and ORF49p. (D) Proteins expressed in rpOkaORF49-41AAAA44-infected MeWo cells (lane 1) and rpOkaORF49-41AAAA44Rev-infected MeWo cells (lane 2) were visualized using Abs against gH, ORF61p, α-tubulin, ORF44p, and ORF49p. (E) The interaction between ORF44p and ORF49p was analyzed in rpOkaORF49-41AAAA44-infected cells (lane 1) and rpOkaORF49-41AAAA44Rev-infected cells (lane 2). Immunoprecipitates obtained using an anti-ORF49 Ab from each type of virus-infected cells were electrophoretically separated and visualized with anti-ORF44 and anti-ORF49 Abs. (F) The viral proteins incorporated into virions from rpOkaORF49-41AAAA44-infected MeWo cells (lane 1), and rpOka-ORF49-41AAAA44-infected MeWoORF49 cells (lane 2) were visualized with Abs against gH, ORF61p, ORF44p, and ORF49p.

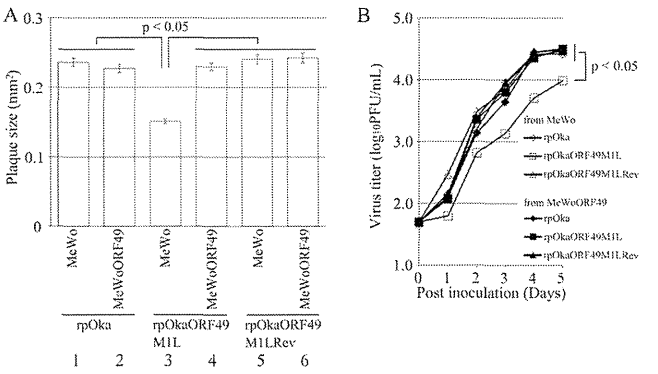

FIG 3 Growth properties of the ORF49M1L mutant virus in MeWo and MeWoORF49 cells. (A) Comparison of plaque sizes among recombinant viruses. MeWo cells or MeWoORF49 cells were infected with rpOka, rpOkaORF49M1L, or rpOkaORF49M1LRev (50 PFU/well) and cultured for 7 days. The infected cells were then stained with an anti-gE Ab, and the plaques were traced and measured by ImageJ software. Plaque size is shown with the standard error of the mean. Statistical significance was determined by Student's *t* test. (B) Growth kinetics of recombinant viruses in MeWo and MeWoORF49 cells. MeWo or MeWoORF49 cells were infected with rpOka, rpOkaORF49M1L, or rpOkaORF49M1LRev (50 PFU/well), harvested at the indicated times, serially diluted, added to newly prepared MeWo cells, and cultured for 5 days. The plaques were stained with an anti-gE Ab and counted. Each point represents the mean titer for two wells of one experiment. The experiments were performed twice independently. Statistical significance was determined by Student's *t* test.

immunoblotting with an anti-ORF44 Ab (Fig. 2A, lanes 3, 4, and 5). ORF44p was coimmunoprecipitated with ORF49p only in cells infected with the wild-type virus, rpOka, or rpOkaORF49M1LRev (data not shown) (Fig. 2B, lane 2) but not in the absence of ORF49p, as seen in rpOkaORF49M1L infection (Fig. 2B, lane 1). Thus, the interaction of ORF44p and ORF49p was specific and conserved in VZV.

ORF44 is essential for viral growth in cell culture. Because ORF49 is completely dispensable for viral reconstitution and propagation in MRC-5 cells, and the interaction between ORF44p and ORF49p was confirmed, we predicted that the ORF44 deletion mutant would be viable at least in MRC-5 cells, despite the fact that loss-of-function analysis showed that it is essential in MeWo cells (5). The ORF44 deletion mutant virus could not be reconstituted from pOka-BACΔ44 (Fig. 1B) in either MeWo cells or MRC-5 cells; however, the revertant virus of pOka-BACΔ44 reconstituted from the pOka-BACΔ44Rev genome (Fig. 1B) showed almost the same plaque size and growth as the parental virus, rpOka, in MeWo cells (data not shown). These findings confirmed that ORF44 is essential for VZV growth in cell culture even in MRC-5 cells.

ORF44p binds to and depends on ORF49p for its accumulation on the TGN in coexpressing cells and infection. When ORF44p was expressed alone by CAG/ORF44 transfection, it was dispersed throughout the cytoplasm and did not localize to the TGN (Fig. 5A). When ORF49p was expressed alone, it was predominantly localized to the juxtanuclear region with TGN46 (Fig. 5B), as reported previously (6). In cells coexpressing ORF44 and ORF49, ORF44p accumulated on the TGN with ORF49p (Fig. 5C), suggesting that the complex formation between ORF44p and ORF49p required no other viral factors and that it functioned in the accumulation of the ORF44p on the TGN. The expression of and interaction

TABLE 2 Comparison of cell-free virus titer and plaque formation

Virus	Cells for: Propagation	Titration	Titer (PFU/ml)[a]	Mean (SE) plaque size, mm²[b]
rpOka	MeWo	MeWo	2.3×10^3	0.232 (0.00891)
	MeWo	MeWoORF49	4.1×10^3	0.225 (0.00854)
	MeWoORF49	MeWo	4.0×10^3	0.232 (0.00911)
	MeWoORF49	MeWoORF49	1.3×10^3	0.206 (0.00828)
rpOkaORF49M1L	MeWo	MeWo	1.5×10^2	0.161 (0.00601)
	MeWo	MeWoORF49	1.7×10^2	0.235 (0.01319)
	MeWoORF49	MeWo	4.0×10^3	0.147 (0.00534)
	MeWoORF49	MeWoORF49	6.3×10^3	0.228 (0.01474)
rpOkaORF49-41AAAA44	MeWo	MeWo	1.2×10^2	0.141 (0.00726)
	MeWo	MeWoORF49	1.3×10^2	0.212 (0.00669)
	MeWoORF49	MeWo	2.1×10^3	0.149 (0.00796)
	MeWoORF49	MeWoORF49	4.7×10^3	0.227 (0.00740)

[a] Titers of cell free viruses are shown from one experiment performed in duplicate.
[b] Plaque sizes are shown as means (standard errors [SE]) from one experiment performed in duplicate.

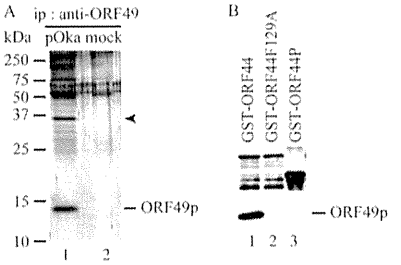

FIG 4 Identification of ORF44p as the binding partner of ORF49p by proteomic analysis and their *in vitro* binding assay. (A) pOka-infected MeWo cells expanded by cell-to-cell spread with full CPE at 2 to 3 days postinfection were lysed with RIPA buffer, and the binding molecules were coimmunoprecipitated with ORF49p using an anti-ORF49 Ab (lane 1). Mock-infected MeWo cells were used as a negative control (lane 2). The immunoprecipitates (ip) were electrophoretically separated and visualized by silver staining. (B) ORF49p expressed in and purified from MeWo cells was incubated with purified GST-ORF44 (lane 1), GST-ORF44F129A (lane 2), or GST-ORF44P (lane 3). Bound proteins were electrophoretically separated and visualized by anti-GST Abs (upper panel) and anti-ORF49 Abs (lower panel).

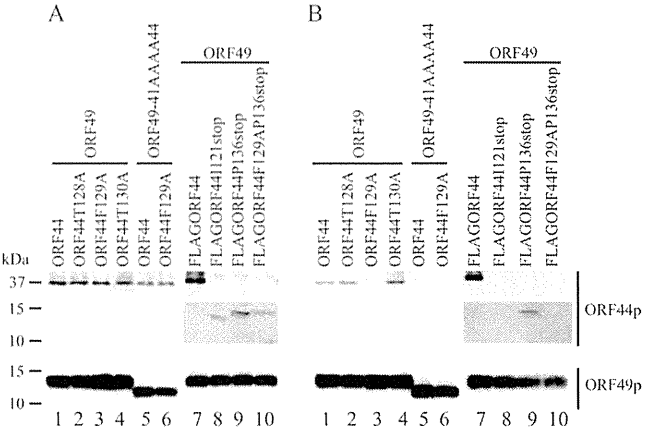

FIG 6 Expression and interaction of ORF44p and ORF49p in cotransfected cells. MeWo cells were cotransfected with CAG/ORF49 (lanes 1 to 4 and 7 to 10) or CAG/ORF49-41AAAA44 (lanes 5 and 6) and CAG/ORF44 (lanes 1 and 5), CAG/ORF44T128A (lane 2), CAG/ORF44F129A (lanes 3 and 6), CAG/ORF44K130A (lane 4), CAG/FLAGORF44 (lane 7), CAG/FLAGORF44I121stop (lane 8), CAG/FLAGORF44P136stop (lane 9), or CAG/FLAGORF44F129AP136stop (lane 10) (A and B). Protein expression was visualized with anti-ORF44p and anti-ORF49p antibodies (A), and proteins immunoprecipitated by anti-ORF49 Ab from cotransfected cells were electrophoretically separated and visualized using anti-ORF44 and anti-ORF49 Abs (B).

between ORF44p and ORF49p were confirmed by immunoblotting with the corresponding Abs and immunoprecipitation with anti-ORF49 Ab followed by immunoblotting with each Ab (Fig. 6A, lane 1, and B, lane 1, respectively). In rpOkaORF49M1LRev-infected MeWo cells, in spite of the broadly diffuse pattern seen for ORF44p, it appeared to accumulate on the TGN with ORF49p (Fig. 7B), as was seen in coexpressing cells (Fig. 5C), and this pattern was also observed in cells infected with rpOka (data not shown). In rpOkaORF49M1L-infected cells, ORF44p was dispersed as in cells expressing ORF44 alone and was not accumulated on the TGN (Fig. 7A), again indicating that the accumulation of ORF44p on the TGN depended on ORF49p and required no other viral factors.

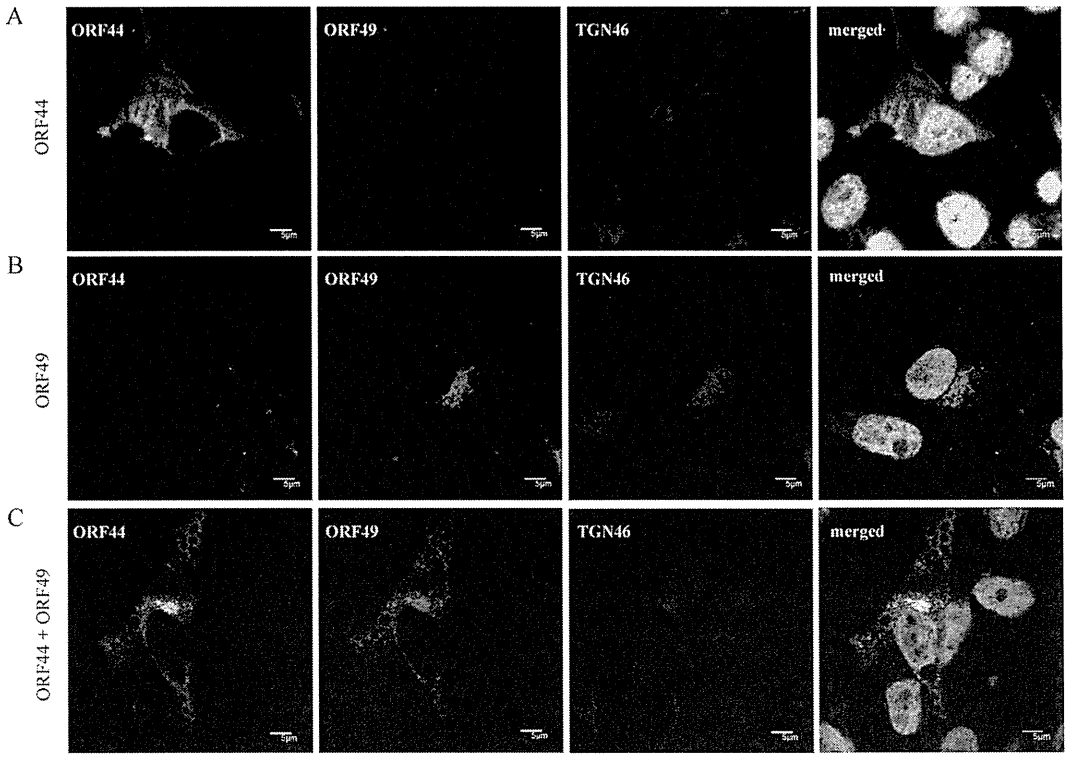

FIG 5 Localization of ORF44p and ORF49p in transiently transfected MeWo cells. MeWo cells were transfected with CAG/ORF44 (A) or CAG/ORF49 (B) or cotransfected with CAG/ORF44 and CAG/ORF49 (C). Cells were fixed at 48 h posttransfection and triple labeled for ORF44p (green), ORF49p (red), and TGN46 (blue). Nuclei were stained with Hoechst 33342 (cyan). Scale bars, 5 μm.

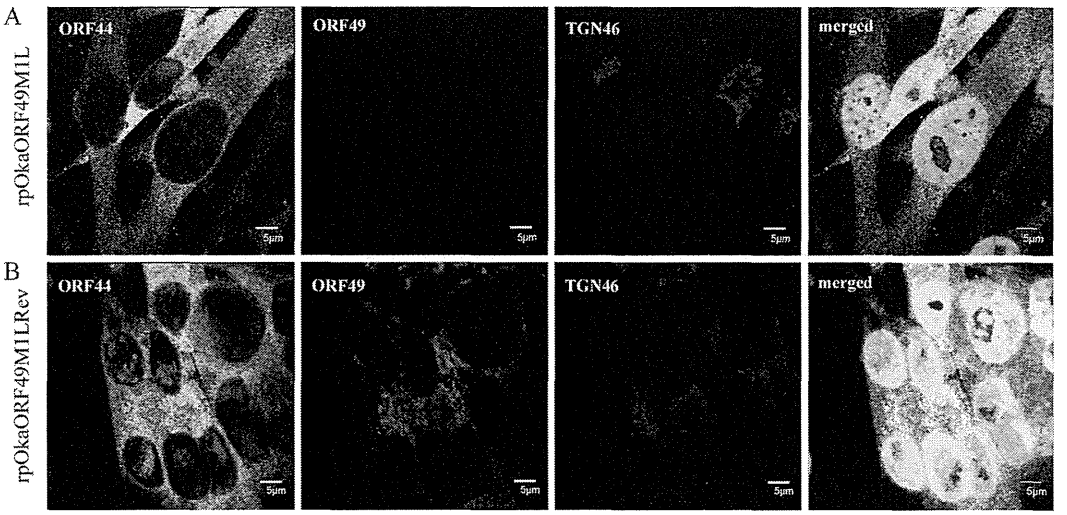

FIG 7 Localization of ORF44p and ORF49p in rpOkaORF49M1L-infected MeWo cells. rpOkaORF49M1L-infected (A) and rpOkaORF49M1LRev-infected (B) MeWo cells were fixed at 48 hpi and triple labeled for ORF44p (green), ORF49p (red), and TGN46 (blue). Nuclei were stained with Hoechst 33342 (cyan). Scale bars, 5 μm.

The phenylalanine at amino acid position 129 of ORF44p functions in the conserved interaction and is essential for VZV infection. In the process of ORF44 cloning, one mutant showed a T-to-C substitution at nt 385, which led to a phenylalanine-to-serine transition at aa 129 (F129S). In cells coexpressing ORF44F129Sp and ORF49p, ORF44F129Sp did not accumulate on the TGN and was not coimmunoprecipitated with ORF49p (data not shown).

To examine whether 129F functions specifically in the conserved interaction in VZV, alanine scanning was performed around 129F (Fig. 1B). ORF44T128Ap, ORF44F129Ap, and ORF44K130Ap showed similar distributions, and none of these mutants localized to the TGN when expressed alone (data not shown), as observed in cells expressing ORF44p alone (Fig. 5A). Coexpression of ORF44T128Ap and ORF44K130Ap with ORF49p (Fig. 8A and C, respectively) resulted in their colocalization with ORF49p at the TGN, as observed in cells coexpressing ORF44p and ORF49p (Fig. 5C). In contrast, ORF44F129Ap was dispersed throughout the cytoplasm and failed to accumulate on the TGN, even when coexpressed with ORF49p (Fig. 8B). The levels of expression of ORF44T128Ap, ORF44F129Ap, and ORF44K130Ap were almost equal (Fig. 6A, lanes 2, 3, and 4, respectively), and ORF44T128Ap and ORF44K130Ap were coimmunoprecipitated with ORF49p (Fig. 6B, lanes 2 and 4, respectively), whereas ORF44F129Ap was not coimmunoprecipitated with ORF49p (Fig. 6B, lane 3).

The results for F129S and F129A suggest that the binding site for ORF49p might reside in an N-terminal domain, as was recently reported for the pUL16 of HSV-1 (26). Therefore, stop codons were inserted at positions to either side of codon 129F (i.e., at I121stop and P136stop). In addition, a construct containing both the F129A and P136stop mutations was made (Fig. 1B). All three mutants were expressed at their predicted size (Fig. 6A, lanes 8, 9, and 10), and only the ORF44P136stop protein was coimmunoprecipitated with ORF49p (Fig. 6B, lane 9), whereas the ORF44I121stop and ORF44F129AP136stop proteins were not (Fig. 6B, lanes 8 and 10, respectively). Consistent with this, only the ORF44P136stop protein accumulated on the TGN with ORF49p (Fig. 8E), and the other two mutants did not (Fig. 8D and F), despite the diffused cytoplasmic localization of all mutants if expressed alone (data not shown). These results show that the binding site for ORF49p resides in the first third of ORF44p and that 129F plays a critical role in binding, either directly or indirectly. Furthermore, in GST-pulldown assays using GST-ORF44 (corresponding to aa 2 to 363), GST-ORF44F129A (aa 2 to 363 with F129A mutation), and GST-ORF44P (aa 180 to 363), only GST-ORF44 pulled down ORF49p expressed in and purified from MeWo cells (Fig. 4B), suggesting that there may not be a binding site within the C-terminal half of ORF44p; however, other C-terminal constructs have not been tested in this or other assays.

To analyze the impact of the 129F mutation in the context of infection, pOka-BACORF44T128A, pOka-BACORF44F129A, pOka-BACORF44K130A, and the revertant BAC for pOka-BACORF44F129A, pOka-BACORF44F129ARev, were generated (Fig. 1B). With the exception of the ORF44F129A mutant, the reconstitution of each virus with a mutation around 129F and of the revertant virus for the F129A mutant was successful, and all of the reconstituted viruses showed similar growth to rpOka (data not shown), suggesting that 129F of ORF44p may play a central role in the function of ORF44p in VZV infection, which occurs through its interaction with ORF49p.

The carboxyl-terminal half of the acidic cluster of ORF49p is required for the conserved interaction with ORF44p. To map the binding domain of ORF49p for ORF44p using the accumulation of ORF44p as an indicator of the interaction, we generated a series of carboxyl-terminal-truncated mutants of ORF49p (Fig. 1C). The coexpression of ORF44p and ORF49N48p or ORF49N44p resulted in the accumulation of ORF44p at the juxtanuclear region with TGN46 and the mutant ORF49p (Fig. 9A and B). In contrast, ORF44p never colocalized with ORF49N40p (Fig. 9C) and was dispersed in the cytoplasm, as when it was expressed alone (Fig. 5A). These results suggested that the ORF44p-binding domain in ORF49p may be located between the aspartate at aa 41 and glutamate at aa 44, which is in the carboxyl-terminal half of the conserved acidic cluster (Fig. 1C) in the ORF49 homologs.

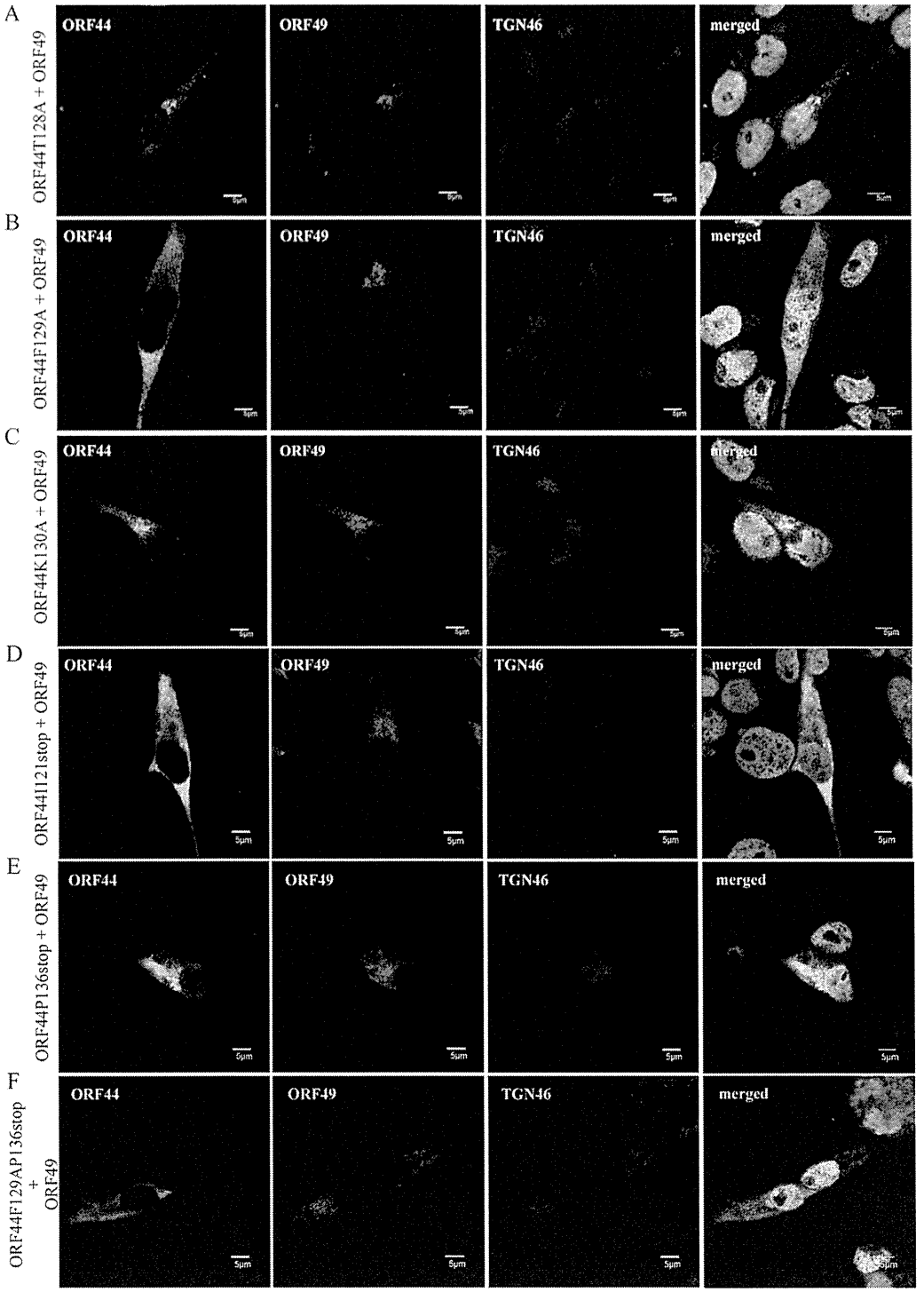

FIG 8 Localization and accumulation of ORF44 mutant proteins in MeWo cells expressing ORF49p. MeWo cells were cotransfected with CAG/ORF49 and CAG/ORF44T128A (A), CAG/ORF44F129A (B), CAG/ORF44K130A (C), CAG/FLAGORF44I121stop (D), CAG/FLAGORF44P136stop (E), or CAG/FLAGORF44F129AP136stop (F). Cells were fixed at 48 h posttransfection and triple labeled for ORF44 (green), ORF49 (red), and TGN46 (blue). Nuclei were stained with Hoechst 33342 (cyan). Scale bars, 5 μm.

To confirm the specificity of the ORF44p and ORF49p interaction while avoiding (although not excluding) nonspecific effects on the function of ORF49p resulting from the destruction of the ORF49p backbone, the four residues (41DFDE44) identified as the candidate ORF44p-binding motif were replaced by alanine, resulting in ORF49-41AAAA44p (Fig. 1C). As shown in Fig. 9D, ORF49-41AAAA44p targeted the TGN, similar to ORF49p (Fig. 5B), but it was unable to accumulate ORF44p on the TGN (Fig. 9E).

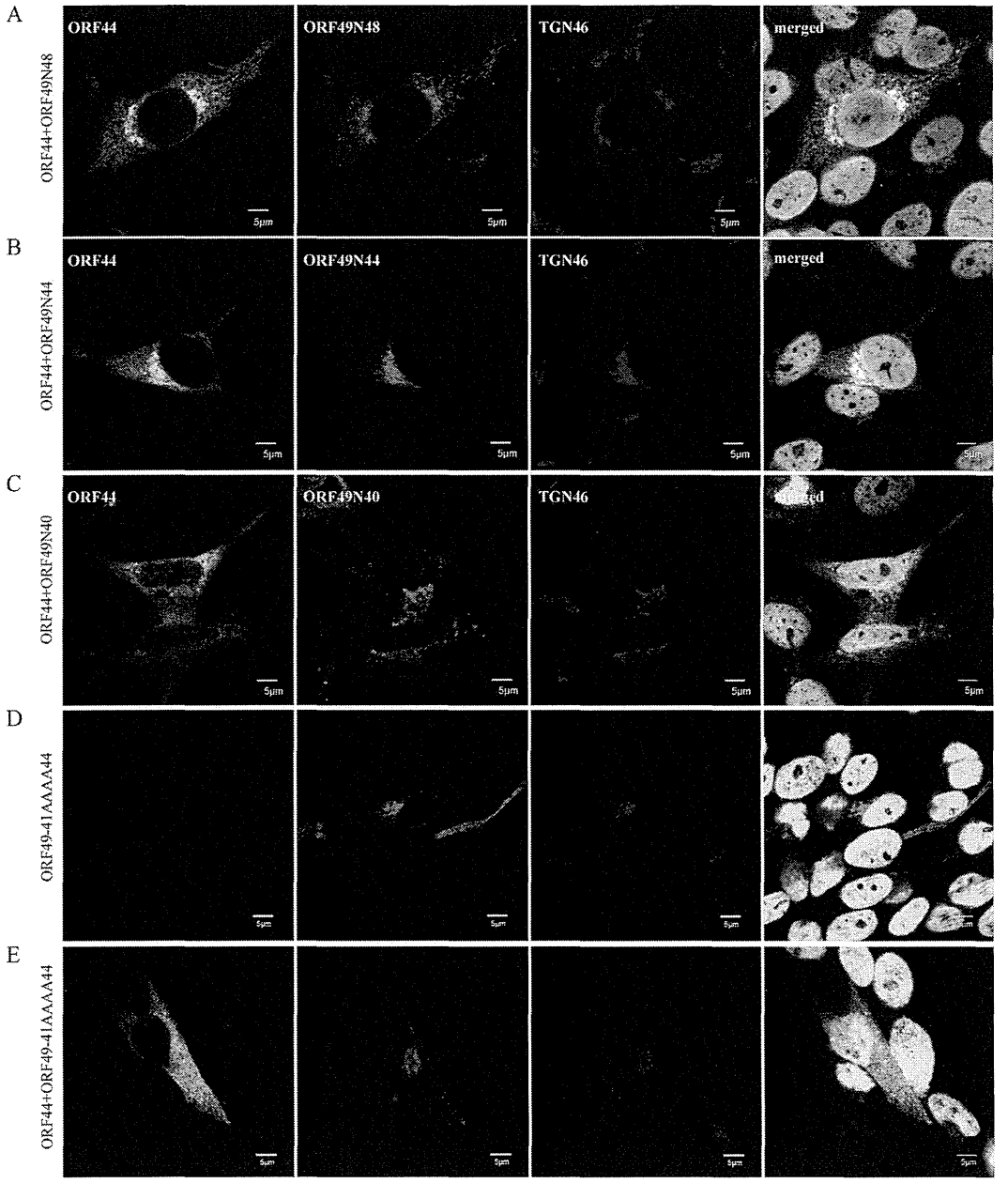

FIG 9 Localization and accumulation of ORF44p in MeWo cells expressing ORF49 mutant proteins. MeWo cells were cotransfected with CAG/ORF44 and CAG/ORF49N48 (A), CAG/ORF49N44 (B), CAG/ORF49N40 (C), or CAG/ORF49-41AAAA44 (E), or transfected with CAG/ORF49-41AAAA44 alone (D). Cells were fixed at 48 h posttransfection and triple labeled for ORF44 (green), ORF49 (red), and TGN46 (blue). Nuclei were stained with Hoechst 33342 (cyan). Scale bars, 5 μm.

Furthermore, ORF49-41AAAA44p did not form a complex with ORF44p or ORF44F129Ap (Fig. 6B, lane 5 or 6) despite the efficient coexpression of all proteins (Fig. 6A, lanes 5 and 6).

The carboxyl-terminal half of the acidic cluster of ORF49p plays a central role in the function of ORF49p during infection. rpOkaORF49-41AAAA44 showed almost the same phenotype as rpOkaORF49M1L, including the loss of the interaction with ORF44p (Fig. 2E, lane 1), the dispersed localization of ORF44p without accumulation on the TGN (Fig. 10A), impaired growth as assessed by plaque size and infectious-center assays (Fig. 11A and B, respectively), and reduced production of infectious progeny virus (to 3 to 10% of the wild-type level [Table 2]), excluding the apparent ORF49-41AAAA44p expression (Fig. 2D, lane 1, and Fig. 10A). These defects were completely rescued by revertant virus infection (Fig. 2D and E, lanes 2, Fig. 10B, and Fig. 11A and B) or by exogenous ORF49p in MeWoORF49 cells (Fig. 11A and B and Table 2). The expression of ORF49-41AAAA44p was detected as a faint and faster-migrating band than that of ORF49p in the revertant virus infection, but an equal amount of ORF44p was detected in both viruses with gH and ORF61p (Fig. 2D, lanes 1 and 2). Furthermore, whereas the interaction between ORF49-41AAAA44p and ORF44p was not detected at all (Fig. 2E, lane 1),

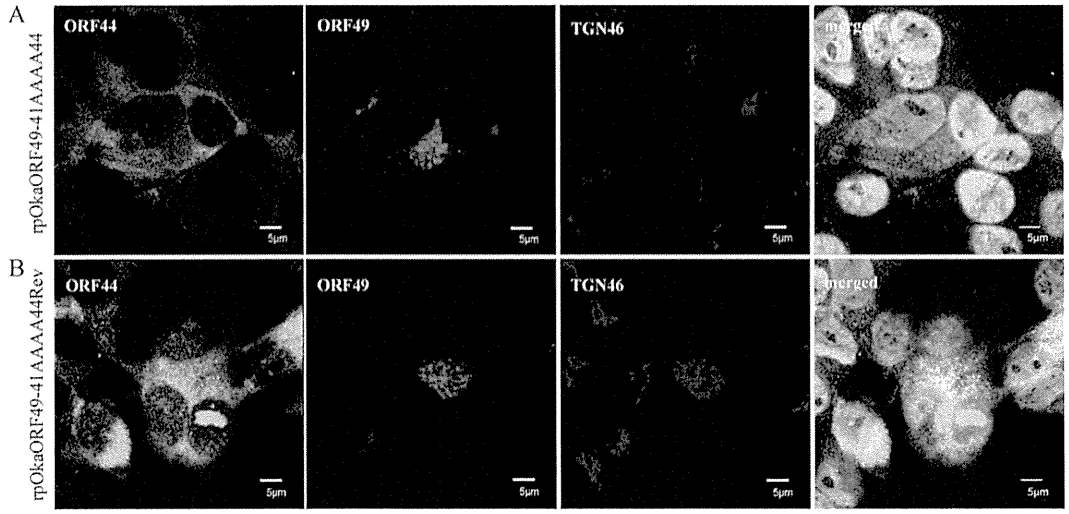

FIG 10 Localization of ORF44p and ORF49p in rpOkaORF49-41AAAA44-infected MeWo cells. rpOkaORF49-41AAAA44-infected MeWo cells (A) and rpOkaORF49-41AAAA44Rev-infected MeWo cells (B) were fixed at 48 hpi and triple labeled for ORF44p (green), ORF49p (red), and TGN46 (blue). Nuclei were stained with Hoechst 33342 (cyan). Scale bars, 5 μm.

ORF44p was incorporated into the rpOkaORF49-41AAAA44 particles in the absence or presence of exogenous ORF49p (Fig. 2F, lane 1 or 2), which was also the case in rpOkaORF49M1L infection (Fig. 2D and F).

Taken together, our results indicated that ORF49p functions in the efficient production of progeny viruses required for VZV infection through its interaction with the essential protein ORF44p.

DISCUSSION

In VZV, ORF49 encodes a nonessential tegument protein that is one of the cell-tropic factors in cell culture (6). In human fetal lung fibroblast MRC-5 cells, the growth of ORF49-defective virus is identical to that of its parental virus, whereas in the human melanoma MeWo cell line, it shows reduced growth; however, the cell tropism of VZV for these two most permissive cell lines has not been studied. In the previous study, we showed that it is a cell-tropic factor, although the step(s) at which ORF49 functions, including the entry, host gene modulation, viral gene expression, viral particle assembly, or egress, remained unclear. Nevertheless, we showed that it may play an important role in the production of a complete virion (6).

VZV is highly cell associated *in vitro*, producing extremely small amounts of infectious virus even when isolated intracellularly (in a particle-to-PFU ratio that varies from approximately 40,000 to 1,000,000) (39, 40), and the particles detected by electron microscopy (EM) analysis appear to be degraded, even in cells infected by the wild-type virus (41–43). The low infectivity and the presence of few or no infectious particles in the cell culture

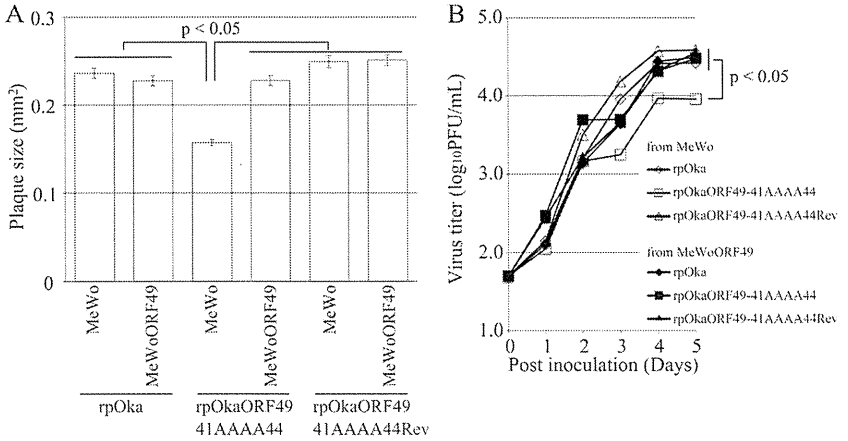

FIG 11 Growth properties of ORF49-41AAAA44 mutant virus in MeWo and MeWoORF49 cells. (A) Comparison of plaque sizes among recombinant viruses. MeWo cells or MeWoORF49 cells were infected with rpOka, rpOkaORF49-41AAAA44, or rpOkaORF49-41AAAA44Rev (50 PFU/well) and cultured for 7 days. Infected cells were stained with an anti-gE Ab, and the plaques were traced and measured by ImageJ software. Plaque size is shown with the standard error of the mean. Statistical significance was determined by Student's *t* test. (B) Growth kinetics of recombinant viruses on MeWo cells and MeWoORF49 cells. MeWo cells or MeWoORF49 cells were infected with rpOka, rpOkaORF49-41AAAA44, or rpOkaORF49-41AAAA44Rev (50 PFU/well), harvested at the indicated times, serially diluted, added to newly prepared MeWo cells, and cultured for 5 days. The plaques were stained with an anti-gE Ab and counted. Each point represents the mean titer for two wells of one experiment. Two experiments were performed independently. Statistical significance was determined by Student's *t* test.

supernatant in VZV have made it difficult to construct a *trans*-complementation system. In such a system, the target viral gene is expressed on permissive cells on which the target gene-deleted virus is only capable of efficient replication similar to the wild-type virus infection on the parental cells. The infection of parental cells by the target gene-deleted virus isolated from cells expressing the target gene enables analysis of its function. This method is useful to confirm that the deletion phenotype is not caused by undesired mutations, which can also be determined by generating the revertant virus to repair the mutated gene within the viral genome. In addition, it can also be used to identify the target gene function, which cannot be determined by simply generating the mutant and revertant viruses and has been used widely in the mutagenic analysis of other herpesviruses, especially in the analysis of structural proteins. However, to the best of our knowledge, this system has been used successfully to analyze gene function in only one report (44) and to confirm that the deletion phenotype is independent of undesired mutation in two reports (45, 46) in VZV research.

In the present study, we established a *trans*-complementation system for ORF49. The ORF49 *trans*-complementation system allowed identification of the precise function of ORF49, which could not be determined by generating its defective virus following EM analysis on MeWo cells. In the EM analysis, no significant differences between the wild-type and ORF49-defective viruses were detected with regard to the intracellular and cell surface viral particle counts or morphology (T. Sadaoka and Y. Mori, unpublished observation), possibly leading to their obvious difference in infectivity, which was reduced by 10-fold or higher in the defective virus. Additionally, in both viruses, the infected cells or viral particles isolated from the same quantity of infected cells contained almost the same amount of viral proteins. The *trans*-complementation system in combination with the results of other analyses described above indicated that ORF49 functions in the production of efficient infectious viruses. The results of EM analysis and immunoblotting suggested that the ORF49 defect did not cause the reduction of viral protein synthesis and viral particle assembly and egress. The cell-free virus titration and plaque formation analyses using the *trans*-complementation system showed that the ORF49p released from the virion into the cells during the entry step was not functional, but *de novo* ORF49p synthesized during lytic replication functioned in the production of efficient infectious virus required for cell-free and cell-to-cell viral transmission modes. However, how the deletion of ORF49 impaired infectivity remained unclear.

To gain further insight into the function of ORF49 during VZV infection, we confirmed ORF44p as its binding partner, as reported in other herpesviruses (12–15), and examined the conserved interaction between these proteins by analyzing their binding properties. We identified 129F in ORF44p as being essential for accumulation on the TGN through the interaction with ORF49p: whether it functions in the binding directly or indirectly is unknown. Simultaneously, 41DFDE44 of the carboxyl-terminal half of the acidic cluster within ORF49p was identified as the binding motif for ORF44p. Among these critical amino acids of ORF44p and ORF49p, each phenylalanine seems to function in the binding. As the phenylalanine is an aromatic and hydrophobic amino acid, it prefers to be buried in protein hydrophobic cores. However, 129F of ORF44p is surrounded by polar amino acid 128T and charged amino acid 130K and 42F of ORF49p by charged amino acids 41D, 43D, and 44E, and there is possibility that these two phenylalanines are exposed at the protein surface. The phenylalanine side chain is fairly nonreactive and is thus rarely directly involved in protein function, although it can play a role in substrate recognition. In particular, hydrophobic amino acids can be involved in binding/recognition of hydrophobic ligands, and the aromatic side chain can also be involved in interactions with other aromatic side chains via stacking interactions (47). In coexpression of ORF44 and ORF49, ORF49F42A mutation alone disrupted the interaction and failed to accumulate ORF44p on the TGN, as seen in ORF49-41AAAA44 mutation, while individual ORF49D41A, -D43A, or -E44A mutation had no effect on them (T. Sadaoka and Y. Mori, unpublished observation). On the other hand, ORF44F129A showed an impaired phenotype in terms of their interaction and its accumulation on the TGN, and neither ORF44T128A nor K130A mutation had any effect on them. However, in the context of infection, ORF49F42A alone could not abrogate the interaction and had no effect on virus growth (T. Sadaoka and Y. Mori, unpublished observation) different from that of ORF49-41AAAA44 mutation (discussed below), while only ORF44F129A was truly lethal for infectious virus production/reconstitution, and again ORF44T128A and ORF44K130A had no effect. These findings may prompt us to conclude that the core machinery of the binding is the noncovalent attractive force between two aromatic rings of phenylalanine and that the additional binding force via charged amino acids around 42F of ORF49p is required in the context of infection; however, there is another possibility—that the ORF44F129A mutation just disrupts the protein structure itself, leading to the loss of interaction. As mentioned above, phenylalanine prefers to be buried in protein hydrophobic cores, and the interaction among the aromatic residues is also important in the protein folding and the structural stabilization of protein (48, 49). Our results about the interaction property revealed that the binding domain within ORF44p is located at the first 136 residues and 129F is essentially involved in the binding, but could not be determined as the precise binding domain, and at the same time, there was no apparent degradation or lower expression of ORF44F129Ap in comparison with ORF44p in both prokaryotic expression and eukaryotic expression systems. To address these issues, further analyses by making an N-terminal truncation for refining the interaction domain and another 129F substitution with tyrosine, which differs only in that it contains a hydroxyl group in place of the ortho hydrogen on the benzene ring, for more preferable substitution to maintain structural stability will be helpful and ongoing.

Assessment of the function of ORF44 in the context of infection did not reveal new findings, with the exception of the F129A mutant, which showed the same phenotype as the deletion mutant. The ORF44 deletion and F129A mutation were lethal for progeny virus production/reconstitution in MeWo and MRC-5 cells; however, an effective *trans*-complementation system for ORF44 as for ORF49 was not successfully established, and at what step(s) in the lytic infection ORF44 essentially functions remained unclear. To find the nonessential but important functions of ORF44 in the context of infection, we turned back to analyzing the ORF49 function by generating ORF49-41AAAA44 virus, in which ORF49p specifically lost the interaction with ORF44p, following comparison of the phenotype between ORF49-defective virus and ORF49-41AAAA44 virus. The rpOkaORF49-41AAAA44 virus showed the same phenotype as the rpOkaORF49M1L virus, indicating that the function of ORF49p in the efficient production of

progeny viruses was completely dependent on the interaction with ORF44p at 41DFDE44. These results suggest that ORF44p is fully functional only in the presence of ORF49p and vice versa and has essential functions during infection, which are independent of the interaction with ORF49p or redundantly supported by other viral factors in the absence of ORF49p.

In the absence of the interaction with ORF49p during infection, ORF44p was detected throughout the cytoplasm and rarely colocalized with the TGN (or with a reorganized organ containing TGN-derived membranes known to be induced by viral infection, although it has not been found in VZV infection), the recognized site of viral assembly; however, incorporation of ORF44p into viral particles was comparable to that observed in wild-type virus infection. These results indicate that ORF44p was not directly incorporated into the particles through the TGN via its interaction with ORF49p, at least in the absence of ORF49p. In HSV-1, the amount of pUL16 packaged into the viral particles was severely reduced in the absence of pUL11 (50), but there are some other interaction partners that potentially function in incorporating pUL16 into the viral particles (i.e., pUL21 and glycoprotein E) (51, 52). In VZV, by global screening using the yeast two-hybrid system, some candidates for ORF44p binding partner have been reported (28, 29), but in our observations, none of these viral proteins other than ORF49p could accumulate ORF44p on the TGN; one viral protein could alter the localization of ORF44p into the nucleus; however, whether it functions in the incorporation of ORF44p into the viral particles remained unclear (T. Sadaoka and Y. Mori, unpublished observation). Anyway, additional ORF44p binding partners active during either the wild-type virus or ORF49-defective virus infection remain to be identified so far, and the complexity of the herpesvirus protein-protein network requires a solid approach to elucidate the essential roles of ORF44 during viral infection further through the interactions with other viral proteins.

In summary, in the present study, we established a *trans*-complementation system for ORF49 and identified ORF44p as the binding partner for ORF49p. We showed that (i) ORF49p functions in the efficient production of infectious virus, (ii) no other viral factor is required for binding, (iii) residue 129F of ORF44p is critical not only for binding to ORF49p but also for progeny virus production/reconstitution, (iv) the carboxyl-terminal half of the acidic cluster (41DFDE44) of ORF49p is the binding motif for ORF44p, and (v) the efficient production of infectious progeny virus by ORF49p is dependent on its interaction with ORF44p. Further analyses of the role of ORF44 mediated by its interaction with ORF49 or other as yet unidentified viral proteins may shed light on the conserved infection mechanisms of the *Herpesvirinae* and those unique to VZV.

ACKNOWLEDGMENTS

We thank Eiko Moriishi (National Institute of Biomedical Innovation, Osaka, Japan) for technical assistance, Panayiotis A. Ioannou (Cell and Gene Therapy Research Group, The Murdoch Children's Research Institute, The University of Melbourne, Royal Children's Hospital, Melbourne, Australia) for providing pGETrec, Wilfried Wackernagel (Genetics, Department of Biology and Environmental Sciences, Universität Oldenburg, Germany) for pCP20, Jun-ichi Miyazaki (Division of Stem Cell Regulation Research, Osaka University Graduate School of Medicine, Japan) for pCAGGS, Masaru Okabe (Department of Experimental Genome Research, Genome Information Research Center, Osaka University, Japan) for pCX-Cre, and Ulrich H. Koszinowski (Max von Pettenkofer Institut fur Virologie, Ludwig-Maximilians-Universität München, Germany) for pHA2 and pST76A-SR.

This study was supported in part by a Grant-in-Aid for Scientific Research on Priority Areas (21022031 to Y.M.) from the Ministry of Education, Culture, Sports, Science, and Technology (MEXT) of Japan, a Grant-in-Aid for Scientific Research (B) (20390138 to Y.M.), a Grant-in-Aid for Young Scientists (B) (20790363 and 22790432 to T.S.), a Grant-in-Aid for Scientific Research (C) (24590551 to T.S.) from the Japan Society for the Promotion of Science (JSPS), and a grant from the Uehara Memorial Foundation (to T.S.).

REFERENCES

1. **Moffat J, Ku CC, Zerboni L, Sommer M, Arvin A.** 2007. VZV: pathogenesis and the disease consequences of primary infection, p 675–688. *In* Arvin A, Campadelli-Fiume G, Mocarski E, Moore PS, Roizman B, Whitley R, Yamanishi K (ed), Human herpesviruses: biology, therapy, and immunoprophylaxis. Cambridge University Press, Cambridge, United Kingdom.
2. **Baines JD, Pellett PE.** 2007. Genetic comparison of human alphaherpesvirus genomes, p 61–69. *In* Arvin A, Campadelli-Fiume G, Mocarski E, Moore PS, Roizman B, Whitley R, Yamanishi K (ed), Human herpesviruses: biology, therapy, and immunoprophylaxis. Cambridge University Press, Cambridge, United Kingdom.
3. **Davison AJ, Scott JE.** 1986. The complete DNA sequence of varicella-zoster virus. J. Gen. Virol. **67**:1759–1816. http://dx.doi.org/10.1099/0022-1317-67-9-1759.
4. **Davison AJ.** 2007. Comparative analysis of the genomes, p 10–26. *In* Arvin A, Campadelli-Fiume G, Mocarski E, Moore PS, Roizman B, Whitley R, Yamanishi K (ed), Human herpesviruses: biology, therapy, and immunoprophylaxis. Cambridge University Press, Cambridge, United Kingdom.
5. **Zhang Z, Selariu A, Warden C, Huang G, Huang Y, Zaccheus O, Cheng T, Xia N, Zhu H.** 2010. Genome-wide mutagenesis reveals that ORF7 is a novel VZV skin-tropic factor. PLoS Pathog. **6**:e1000971. http://dx.doi.org/10.1371/journal.ppat.1000971.
6. **Sadaoka T, Yoshii H, Imazawa T, Yamanishi K, Mori Y.** 2007. Deletion in open reading frame 49 of varicella-zoster virus reduces virus growth in human malignant melanoma cells but not in human embryonic fibroblasts. J. Virol. **81**:12654–12665. http://dx.doi.org/10.1128/JVI.01183-07.
7. **Baines JD, Jacob RJ, Simmerman L, Roizman B.** 1995. The herpes simplex virus 1 UL11 proteins are associated with cytoplasmic and nuclear membranes and with nuclear bodies of infected cells. J. Virol. **69**:825–833.
8. **Britt WJ, Jarvis M, Seo JY, Drummond D, Nelson J.** 2004. Rapid genetic engineering of human cytomegalovirus by using a lambda phage linear recombination system: demonstration that pp28 (UL99) is essential for production of infectious virus. J. Virol. **78**:539–543. http://dx.doi.org/10.1128/JVI.78.1.539-543.2004.
9. **Silva MC, Yu QC, Enquist L, Shenk T.** 2003. Human cytomegalovirus UL99-encoded pp28 is required for the cytoplasmic envelopment of tegument-associated capsids. J. Virol. **77**:10594–10605. http://dx.doi.org/10.1128/JVI.77.19.10594-10605.2003.
10. **MacLean CA, Dolan A, Jamieson FE, McGeoch DJ.** 1992. The myristylated virion proteins of herpes simplex virus type 1: investigation of their role in the virus life cycle. J. Gen. Virol. **73**:539–547. http://dx.doi.org/10.1099/0022-1317-73-3-539.
11. **Silva MC, Schroer J, Shenk T.** 2005. Human cytomegalovirus cell-to-cell spread in the absence of an essential assembly protein. Proc. Natl. Acad. Sci. U. S. A. **102**:2081–2086. http://dx.doi.org/10.1073/pnas.0409597102.
12. **Loomis JS, Courtney RJ, Wills JW.** 2003. Binding partners for the UL11 tegument protein of herpes simplex virus type 1. J. Virol. **77**:11417–11424. http://dx.doi.org/10.1128/JVI.77.21.11417-11424.2003.
13. **Guo H, Wang L, Peng L, Zhou ZH, Deng H.** 2009. Open reading frame 33 of a gammaherpesvirus encodes a tegument protein essential for virion morphogenesis and egress. J. Virol. **83**:10582–10595. http://dx.doi.org/10.1128/JVI.00497-09.
14. **Liu Y, Cui Z, Zhang Z, Wei H, Zhou Y, Wang M, Zhang XE.** 2009. The tegument protein UL94 of human cytomegalovirus as a binding partner for tegument protein pp28 identified by intracellular imaging. Virology **388**:68–77. http://dx.doi.org/10.1016/j.virol.2009.03.007.
15. **Maninger S, Bosse JB, Lemnitzer F, Pogoda M, Mohr CA, von Einem J, Walther P, Koszinowski UH, Ruzsics Z.** 2011. M94 is essential for the

secondary envelopment of murine cytomegalovirus. J. Virol. 85:9254–9267. http://dx.doi.org/10.1128/JVI.00443-11.
16. Meckes DG, Jr, Wills JW. 2007. Dynamic interactions of the UL16 tegument protein with the capsid of herpes simplex virus. J. Virol. 81:13028–13036. http://dx.doi.org/10.1128/JVI.01306-07.
17. Nalwanga D, Rempel S, Roizman B, Baines JD. 1996. The UL 16 gene product of herpes simplex virus 1 is a virion protein that colocalizes with intranuclear capsid proteins. Virology 226:236–242. http://dx.doi.org/10.1006/viro.1996.0651.
18. Oshima S, Daikoku T, Shibata S, Yamada H, Goshima F, Nishiyama Y. 1998. Characterization of the UL16 gene product of herpes simplex virus type 2. Arch. Virol. 143:863–880. http://dx.doi.org/10.1007/s007050050338.
19. Yeh PC, Meckes DG, Jr, Wills JW. 2008. Analysis of the interaction between the UL11 and UL16 tegument proteins of herpes simplex virus. J. Virol. 82:10693–10700. http://dx.doi.org/10.1128/JVI.01230-08.
20. Johnson DC, Baines JD. 2011. Herpesviruses remodel host membranes for virus egress. Nat. Rev. Microbiol. 9:382–394. http://dx.doi.org/10.1038/nrmicro2559.
21. Baines JD, Roizman B. 1991. The open reading frames UL3, UL4, UL10, and UL16 are dispensable for the replication of herpes simplex virus 1 in cell culture. J. Virol. 65:938–944.
22. Dunn W, Chou C, Li H, Hai R, Patterson D, Stolc V, Zhu H, Liu F. 2003. Functional profiling of a human cytomegalovirus genome. Proc. Natl. Acad. Sci. U. S. A. 100:14223–14228. http://dx.doi.org/10.1073/pnas.2334032100.
23. Klupp BG, Bottcher S, Granzow H, Kopp M, Mettenleiter TC. 2005. Complex formation between the UL16 and UL21 tegument proteins of pseudorabies virus. J. Virol. 79:1510–1522. http://dx.doi.org/10.1128/JVI.79.3.1510-1522.2005.
24. Phillips SL, Bresnahan WA. 2012. The human cytomegalovirus (HCMV) tegument protein UL94 is essential for secondary envelopment of HCMV virions. J. Virol. 86:2523–2532. http://dx.doi.org/10.1128/JVI.06548-11.
25. Yu D, Silva MC, Shenk T. 2003. Functional map of human cytomegalovirus AD169 defined by global mutational analysis. Proc. Natl. Acad. Sci. U. S. A. 100:12396–12401. http://dx.doi.org/10.1073/pnas.1635160100.
26. Chadha P, Han J, Starkey JL, Wills JW. 2012. Regulated interaction of tegument proteins UL16 and UL11 from herpes simplex virus. J. Virol. 86:11886–11898. http://dx.doi.org/10.1128/JVI.01879-12.
27. Phillips SL, Cygnar D, Thomas A, Bresnahan WA. 2012. Interaction between the human cytomegalovirus tegument proteins UL94 and UL99 is essential for virus replication. J. Virol. 86:9995–10005. http://dx.doi.org/10.1128/JVI.01078-12.
28. Stellberger T, Hauser R, Baiker A, Pothineni VR, Haas J, Uetz P. 2010. Improving the yeast two-hybrid system with permutated fusions proteins: the varicella zoster virus interactome. Proteome Sci. 8:8. http://dx.doi.org/10.1186/1477-5956-8-8.
29. Uetz P, Dong YA, Zeretzke C, Atzler C, Baiker A, Berger B, Rajagopala SV, Roupelieva M, Rose D, Fossum E, Haas J. 2006. Herpesviral protein networks and their interaction with the human proteome. Science 311:239–242. http://dx.doi.org/10.1126/science.1116804.
30. Sadaoka T, Yanagi T, Yamanishi K, Mori Y. 2010. Characterization of the varicella-zoster virus ORF50 gene, which encodes glycoprotein M. J. Virol. 84:3488–3502. http://dx.doi.org/10.1128/JVI.01838-09.
31. Niwa H, Yamamura K, Miyazaki J. 1991. Efficient selection for high-expression transfectants with a novel eukaryotic vector. Gene 108:193–199. http://dx.doi.org/10.1016/0378-1119(91)90434-D.
32. Sadaoka T, Yamanishi K, Mori Y. 2006. Human herpesvirus 7 U47 gene products are glycoproteins expressed in virions and associate with glycoprotein H. J. Gen. Virol. 87:501–508. http://dx.doi.org/10.1099/vir.0.81374-0.
33. Okuno T, Yamanishi K, Shiraki K, Takahashi M. 1983. Synthesis and processing of glycoproteins of varicella-zoster virus (VZV) as studied with monoclonal antibodies to VZV antigens. Virology 129:357–368. http://dx.doi.org/10.1016/0042-6822(83)90175-7.
34. Nagaike K, Mori Y, Gomi Y, Yoshii H, Takahashi M, Wagner M, Koszinowski U, Yamanishi K. 2004. Cloning of the varicella-zoster virus genome as an infectious bacterial artificial chromosome in Escherichia coli. Vaccine 22:4069–4074. http://dx.doi.org/10.1016/j.vaccine.2004.03.062.
35. Narayanan K, Williamson R, Zhang Y, Stewart AF, Ioannou PA. 1999. Efficient and precise engineering of a 200 kb beta-globin human/bacterial artificial chromosome in E. coli DH10B using an inducible homologous recombination system. Gene Ther. 6:442–447. http://dx.doi.org/10.1038/sj.gt.3300901.
36. Cherepanov PP, Wackernagel W. 1995. Gene disruption in Escherichia coli: TcR and KmR cassettes with the option of Flp-catalyzed excision of the antibiotic-resistance determinant. Gene 158:9–14. http://dx.doi.org/10.1016/0378-1119(95)00193-A.
37. Hobom U, Brune W, Messerle M, Hahn G, Koszinowski UH. 2000. Fast screening procedures for random transposon libraries of cloned herpesvirus genomes: mutational analysis of human cytomegalovirus envelope glycoprotein genes. J. Virol. 74:7720–7729. http://dx.doi.org/10.1128/JVI.74.17.7720-7729.2000.
38. Shevchenko A, Wilm M, Vorm O, Mann M. 1996. Mass spectrometric sequencing of proteins silver-stained polyacrylamide gels. Anal. Chem. 68:850–858. http://dx.doi.org/10.1021/ac950914h.
39. Carpenter JE, Henderson EP, Grose C. 2009. Enumeration of an extremely high particle-to-PFU ratio for varicella-zoster virus. J. Virol. 83:6917–6921. http://dx.doi.org/10.1128/JVI.00081-09.
40. Shiraki K, Takahashi M. 1982. Virus particles and glycoprotein excreted from cultured cells infected with varicella-zoster virus (VZV). J. Gen. Virol. 61:271–275. http://dx.doi.org/10.1099/0022-1317-61-2-271.
41. Gabel CA, Dubey L, Steinberg SP, Sherman D, Gershon MD, Gershon AA. 1989. Varicella-zoster virus glycoprotein oligosaccharides are phosphorylated during posttranslational maturation. J. Virol. 63:4264–4276.
42. Gershon AA, Sherman DL, Zhu Z, Gabel CA, Ambron RT, Gershon MD. 1994. Intracellular transport of newly synthesized varicella-zoster virus: final envelopment in the trans-Golgi network. J. Virol. 68:6372–6390.
43. Harson R, Grose C. 1995. Egress of varicella-zoster virus from the melanoma cell: a tropism for the melanocyte. J. Virol. 69:4994–5010.
44. Ali MA, Li Q, Fischer ER, Cohen JI. 2009. The insulin degrading enzyme binding domain of varicella-zoster virus (VZV) glycoprotein E is important for cell-to-cell spread and VZV infectivity, while a glycoprotein I binding domain is essential for infection. Virology 386:270–279. http://dx.doi.org/10.1016/j.virol.2009.01.023.
45. Tischer BK, Kaufer BB, Sommer M, Wussow F, Arvin AM, Osterrieder N. 2007. A self-excisable infectious bacterial artificial chromosome clone of varicella-zoster virus allows analysis of the essential tegument protein encoded by ORF9. J. Virol. 81:13200–13208. http://dx.doi.org/10.1128/JVI.01148-07.
46. Yamagishi Y, Sadaoka T, Yoshii H, Somboonthum P, Imazawa T, Nagaike K, Ozono K, Yamanishi K, Mori Y. 2008. Varicella-zoster virus glycoprotein M homolog is glycosylated, is expressed on the viral envelope, and functions in virus cell-to-cell spread. J. Virol. 82:795–804. http://dx.doi.org/10.1128/JVI.01722-07.
47. Betts MJ, Russell RB. 22 May 2003. Amino acid properties and consequences of substitutions. Chapter 14. *In* Barnes MR, Gray IC (ed), Bioinformatics for geneticists. Wiley, Chichester, West Sussex, England. http://dx.doi.org/10.1002/0470867302.ch14.
48. Burley SK, Petsko GA. 1985. Aromatic-aromatic interaction: a mechanism of protein structure stabilization. Science 229:23–28. http://dx.doi.org/10.1126/science.3892686.
49. Eidenschink LA, Kier BL, Andersen NH. 2009. Determinants of fold stabilizing aromatic-aromatic interactions in short peptides. Adv. Exp. Med. Biol. 611:73–74. http://dx.doi.org/10.1007/978-0-387-73657-0_32.
50. Meckes DG, Jr, Marsh JA, Wills JW. 2010. Complex mechanisms for the packaging of the UL16 tegument protein into herpes simplex virus. Virology 398:208–213. http://dx.doi.org/10.1016/j.virol.2009.12.004.
51. Han J, Chadha P, Meckes DG, Jr, Baird NL, Wills JW. 2011. Interaction and interdependent packaging of tegument protein UL11 and glycoprotein E of herpes simplex virus. J. Virol. 85:9437–9446. http://dx.doi.org/10.1128/JVI.05207-11.
52. Harper AL, Meckes DG, Jr, Marsh JA, Ward MD, Yeh PC, Baird NL, Wilson CB, Semmes OJ, Wills JW. 2010. Interaction domains of the UL16 and UL21 tegument proteins of herpes simplex virus. J. Virol. 84:2963–2971. http://dx.doi.org/10.1128/JVI.02015-09.

Microbiology and Immunology

Microbiol Immunol 2014; 58: 119–125
doi: 10.1111/1348-0421.12121

ORIGINAL ARTICLE

MHC class I molecules are incorporated into human herpesvirus-6 viral particles and released into the extracellular environment

Megumi Ota[1], Satoshi Serada[2], Tetsuji Naka[2] and Yasuko Mori[1]

[1]Division of Clinical Virology, Center for Infectious Diseases, Kobe University Graduate School of Medicine, 7-5-1, Kusunoki-cho, Chuo-ku, Kobe 650-0017, Japan and [2]Laboratory of Immune Signal, Division of Biomedical Research, National Institute of Biomedical Innovation, 7-6-8, Saito-Asagi, Ibaraki, Osaka 567-0085, Japan

ABSTRACT

Human herpesvirus-6 (HHV-6), which belongs to the betaherpesvirus subfamily, mainly replicates in T lymphocytes. Here, we show that MHC class I molecules are incorporated into HHV-6 viral particles and released into the extracellular environment. In addition, HHV-6A/B-infected T cells showed reduced surface and intracellular expression of MHC class I molecules. The cellular machinery responsible for molecular transport appears to be modified upon HHV-6 infection, causing MHC class I molecules to be transported to virion assembly sites.

Key words human herpesvirus-6A/B, MHC class I, viral particles.

Human herpesvirus 6 (HHV-6), which belongs to the betaherpesvirus subfamily (1), was first isolated from peripheral blood lymphocytes obtained from patients with lymphoproliferative disorders (2). HHV-6 isolates are classified as HHV-6A and HHV-6B based on genetic and antigenic differences and their cell tropism (2–5). Primary infection with HHV-6B causes exanthem subitum (6). The diseases caused by HHV-6A are so far unknown. HHV-6B mostly infects infants and remains latent in more than 90% of the population (7).

In general, herpesviruses use several strategies to evade host immune responses. For example, viruses may inhibit MHC class I-associated antigen presentation to escape detection by cytotoxic T lymphocytes. Several proteins expressed by herpesviruses block the transport of antigenic peptides from the cytosol to the endoplasmic reticulum (8–11), whereas others retain (12–14) or destroy class I molecules, or deliver them to lysosomes for degradation (15–18). The result is reduced surface expression of MHC class I molecules, enabling the virus to evade host immune surveillance.

HHV-6A, but not HHV-6B, downregulates expression of MHC class I in dendritic cells (19). HHV-6 U21 binds to and diverts MHC class I molecules to an endolysosomal compartment, effectively removing them from the cell surface and providing a possible means of immune escape (20).

Here, we show that expression of MHC class I molecules by infected cells is downregulated with incorporation into HHV-6 viral particles, suggesting a possible mechanism by which the virus escapes host immune surveillance.

MATERIALS AND METHODS

Cells and viruses

CBMCs were prepared as described previously (21). CBMCs were provided by K. Adachi (Minoh Hospital, Minoh,

Correspondence
Yasuko Mori, Division of Clinical Virology, Center for Infectious Diseases, Kobe University Graduate School of Medicine, 7-5-1, Kusunoki-cho, Chuo-ku, Kobe 650-0017, Japan.
Tel: +81 78 382 6878; fax: +81 78 382 6879; email: ymori@med.kobe-u.ac.jp

Received 17 October 2013; revised 22 November 2013; accepted 6 December 2013.

List of Abbreviations: CBMC, umbilical cord blood mononuclear cell; LC-MS/MS, liquid chromatography-tandem mass spectrometry; HHV-6A, human herpesvirus-6A; HHV-6B, human herpesvirus-6B; MVB, multivesicular body; TGN, *trans*-Golgi network.

Japan) and H. Yamada (Kobe University Graduate School of Medicine, Kobe, Japan) and purchased from the Cell Bank of the RIKEN BioResource Center, Tsukuba, Japan. Virus stocks were also prepared as described previously (21, 22). HSB-2 and MT-4 cell lines were used in this study (23). HHV-6A (strain GS) and HHV-6B (strain HST) were prepared as previously described (21).

Antibodies

Monoclonal antibody (Mab) OHV-1 (24) and a polyclonal antibody against gB (23, 25) have been described previously. The following other Mabs were purchased: MHC class I (clone: W6/32; Bio Legend, San Diego, CA, USA), CD63 (clone: CLB-gran/12, 435; Sanquin Blood Supply, Amsterdam, the Netherlands), and α-tubulin (clone: B-5-1-2; Sigma, St Louis, MO, USA). The following secondary antibodies were used: Alexa Fluor 488- or 594-conjugated F(ab′)2 fragment of goat anti-mouse or rabbit immunoglobulin G (IgG) (Invitrogen, Tokyo, Japan) and anti-mouse IgG, horseradish peroxidase-linked whole antibody (from sheep) (GE Healthcare, Piscataway, NJ, USA).

Virion and exosome isolation

Virions and exosomes were purified as previously described (23, 26). The collected fractions were used for western blotting, electron microscopy or liquid chromatography-tandem mass spectrometry (LC-MS/MS).

Liquid chromatography-tandem mass spectrometry

The fractions described above were analyzed by LC-MS/MS. Proteins were diluted tenfold with 9.8 M urea. The solutions were adjusted to pH 8.5, reduced with 13 mM dithiothreitol at 37°C for 1.5 hr and alkylated with 27 mM iodoacetamide in the dark for 1 hr. The protein mixtures were further diluted with 100 mM triethylammonium bicarbonate (pH 8.5) to reduce urea to 1 M, and digested with 4 μL of 1 mg/mL trypsin–tosyl phenylalanyl chloromethyl ketone solution. Samples were digested overnight at 37°C. Following digestion, lysates were acidified by adding 10% trifluoroacetic acid. The samples were desalted using peptide cleanup C18 spin tubes (Agilent Technologies, Santa Clara, CA, USA) and vacuum-dried. NanoLC-MS/MS analyses were performed on an LTQ-Orbitrap XL mass spectrometer (Thermo Fisher Scientific, Waltham, MA, USA) as described previously (27), while spray voltage was changed to 1800 V. Peptides and proteins were identified by automated database searches using Proteome Discoverer v.1.1 (Thermo Fisher Scientific) against all entries of the Swiss Prot protein database (version 3.26) with a precursor mass tolerance of 10 p.p.m., a fragment ion mass tolerance of 0.8 Da, and strict trypsin specificity, allowing for up to two missed cleavages. Cysteine carbamidomethylation was set as a fixed modification, and methionine oxidation was allowed as a variable modification.

Western blotting

Western blotting was performed as described previously (28, 29).

Electron microscopy

Electron microscopy was performed as described previously (30).

Briefly, the virion-containing pellets were resuspended in 2% (w/v) paraformaldehyde solution buffered with 0.1 M phosphate (pH 7.2). Next, 5 μL of the resuspended pellet was loaded onto formvar–carbon-coated grids to adsorb the virions. Immunostaining was then performed. The virions were incubated with mouse anti-gB, anti-MHC class I or anti-CD63 antibody for 1 hr at room temperature, followed by goat anti-mouse IgG conjugated to 10 nm colloidal gold particles (GE Healthcare) for a further 1 hr at room temperature. After immunolabeling, the samples were washed in distilled water, stained for 5 min with uranyl oxalate, pH 7.0, washed again, embedded in a mixture of 1.8% methylcellulose and 0.4% uranyl acetate, pH 4.0, at 4°C, air-dried, and observed under a Hitachi H-7100 electron microscope (Hitachi, Tokyo, Japan). For the control experiments, samples were incubated with the secondary antibody alone.

Flow cytometry

MT-4 cells were infected with HHV-6B. At 72 hr post-infection, the cells were fixed with 4% (w/v) paraformaldehyde at room temperature for 15 min and incubated with anti-MHC class I Mab at 37°C for 1 hr. The cells were then stained with an appropriate secondary antibody at 37°C for 30 min. For the control experiments, samples were incubated with the secondary antibody alone. Stained cells were analyzed using a flow cytometer (ec800; Sony, Tokyo, Japan).

Immunofluorescence assay

Immunofluorescence assay was performed as described previously (28). Briefly, MT-4 cells were infected with HHV-6B. At 72 hr post-infection, the cells were fixed with cold acetone–methanol (7:3) and incubated at 37°C

for 1 hr with an anti-HHV-6 gB rabbit antibody or an anti-MHC class I Mab. After washing for 10 min with PBS containing 0.02% Tween-20, the cells were incubated with an appropriate secondary antibody at 37°C for 30 min, followed by Hoechst33342 at 37°C for 40 min. After washing as described above, signals were detected by a confocal laser-scanning microscope (Olympus FluoView FV1000; Olympus, Tokyo, Japan).

RESULTS

Virion and exosome isolation

Extracellular viral particles containing exosomes were purified from the culture supernatant of HHV-6A (strain GS)-infected HSB-2 or HHV-6B (strain HST)-infected MT-4 cells. The particle-containing fractions were confirmed by western blotting with an anti-gB antibody (23, 25). Next, the particle-containing fractions were analyzed by LC-MS/MS (27), which detected many cellular proteins (unpublished data). Of the host proteins detected, our analyses focused on MHC class I molecules.

Virion- or exosome-associated fractions contain MHC class I molecules

To verify expression of MHC class I within viral particles, the proteins in fractions 3–10 were separated by SDS–PAGE and analyzed by western blotting with anti-gB rabbit, anti-MHC class I or anti-CD63 antibodies. As shown in Figure 1, gB protein was detected in fractions 5–6 whereas MHC class I was detected primarily in fractions 6–8. We have previously reported that the MVB marker, CD63, is incorporated into virions and exosomes (23); therefore, expression of CD63 was also examined. As expected, CD63 was detected in fractions 5–10 (Fig. 1c). To confirm expression of MHC class I within both virions and exosomes, negative staining of fractions 6 and 7 were performed, followed by electron microscopy (30). Fraction 6 contained mainly viral particles of diameter approximately 200 nm. Both MHC class I (Fig. 1e) and gB protein (Fig. 1d) were present in these particles. Fraction 7 contained mainly exosomes of diameter approximately 50–100 nm (Fig. 1f). These exosomes contained MHC class I, which confirmed the results of the western blotting experiments. Taken together, these results indicate that MHC class I molecules are present in exosomes and virions released from HHV-6B-infected cells.

Downregulated expression of MHC class I molecules on the surface of HHV-6B-infected cells

Downregulation of MHC class I occurs in many different virus-infected cells (31–37). Because MHC class I molecules were incorporated into virions, HHV-6-infected MT-4 cells might show an apparent downregulation in cell surface expression. To confirm this, HHV-6B- or mock-infected cells harvested 72 hr post-infection were fixed and then stained with an anti-MHC class I antibody. Surface expression of MHC class I was then analyzed by flow cytometry. As expected, HHV-6B-infected cells showed downregulated cell surface expression of MHC class I when compared with mock-infected cells (Fig. 2a). This reduced expression was confirmed by western blot analysis (Fig. 2b), indicating that expression of MHC class I molecules within HHV-6-infected cells (not just expression on the cell surface) was also downregulated. Next, the localization of MHC class I molecules in these cells was assessed after they had been fixed and co-stained with anti-MHC class I and gB antibodies. MHC class I in infected cells was localized mainly within intracellular compartments, and colocalized with the envelope glycoprotein gB during the later stages of infection; however, MHC class I was mainly localized to the plasma membrane in mock-infected cells (Fig. 2c).

DISCUSSION

Here, we used mass spectrometry-based proteomics analysis to show that MHC class I molecules are incorporated into HHV-6 viral particles. Downregulation of MHC class I molecules in virus-infected cells is an important mechanism by which viruses evade immune surveillance (31–37). We showed that downregulation of MHC class I molecules occurs in T cells infected by HHV-6. MHC class I molecules are incorporated into viral particles and exosomes and then released into the extracellular environment, suggesting a possible strategy for escaping host immune responses. In addition, MHC class I molecules incorporated into virions and exosomes may assist viral entry. Further studies are needed to address this question.

We have previously reported that immature HHV-6 particles bud into TGN or TGN-derived vesicles (which are produced in HHV-6B-infected cells), that vesicles containing mature virions become MVBs, and that virions and exosomes are released into the extracellular environment via an exosomal secretary pathway (23). It is possible that MHC class I molecules are transported into the TGN-derived membranes from which the virions bud and then incorporated into virions within infected cells without being recycled (Fig. 3).

Within infected cells, MHC class I molecules colocalized with the gB protein in the cytoplasm indicating that, like viral glycoproteins, they are sorted into vesicles. The reduction in the total (both cell surface and

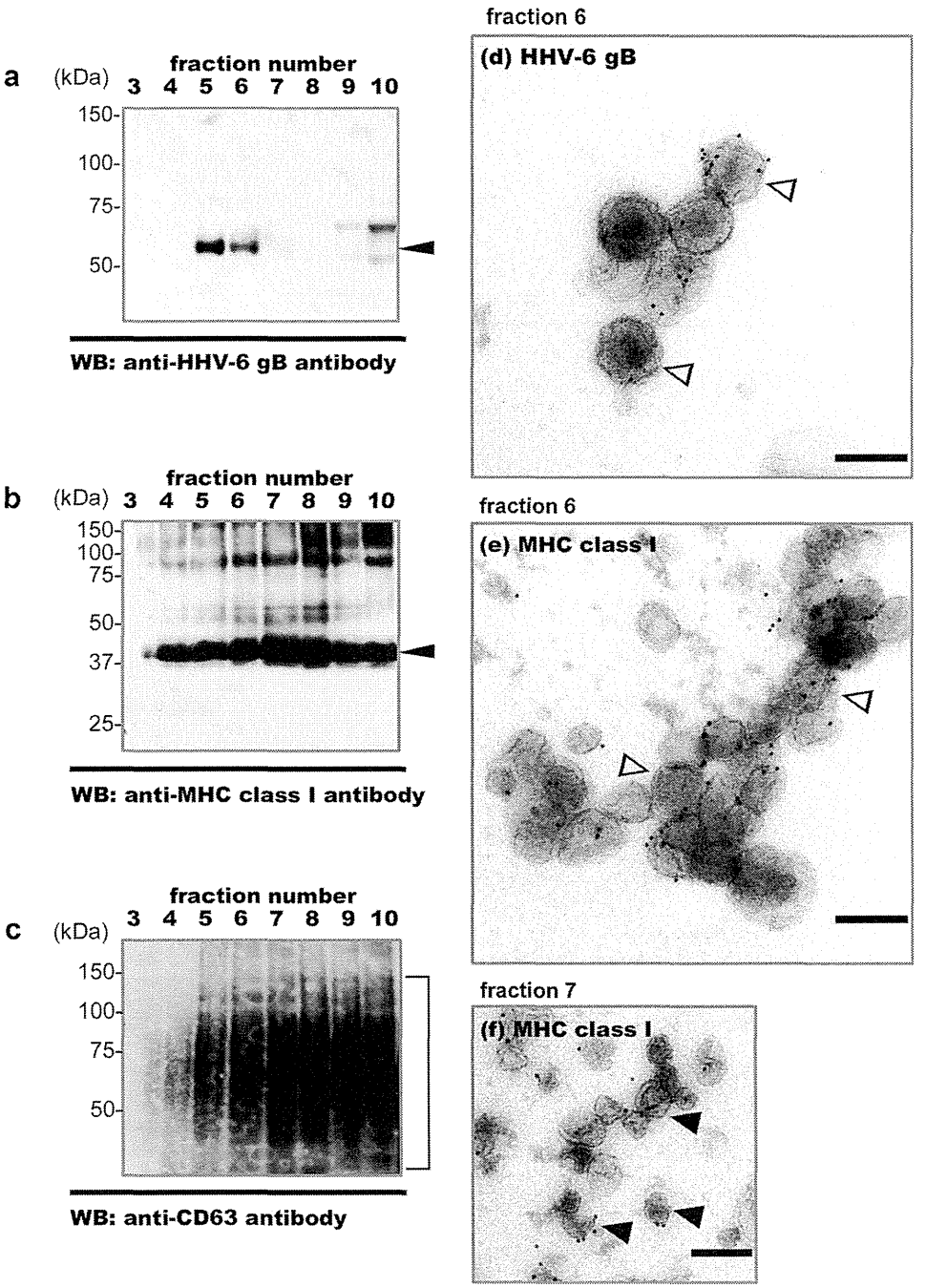

Fig. 1. MHC class I molecules are incorporated into virions and exosomes and released from HHV-6B-infected cells. Virions and exosomes were collected from the culture medium of HHV-6B-infected cells by sucrose density gradient centrifugation and examined by (a–c) western blotting and (d–f) electron microscopy. Western blots with (a) anti-gB rabbit, (b) anti-MHC class I (W6/32) or (c) anti-CD63 (CLB-gran/12, 435) antibodies are shown. The same amount of each protein fraction was added to each well of the gel. Immunogold labeling of (d) gB in fraction 6 and of (e,f) MHC class I in fractions 6 and 7. The fractions were collected from the bottom of tube. Hollow arrowheads, labeled virions; filled arrowheads, exosomes. Scale bars: 200 nm (d–f).

intracellular) expression of MHC class I in HHV-6-infected cells suggests that some of them may be transported to lysosomes and degraded, as this route is the same as that used to transport particles to MVBs.

Although several host proteins are usually expressed on the surfaces of uninfected cells, they are expressed in the same intracellular compartments as those in which viral particles incorporated. Newly formed compartments

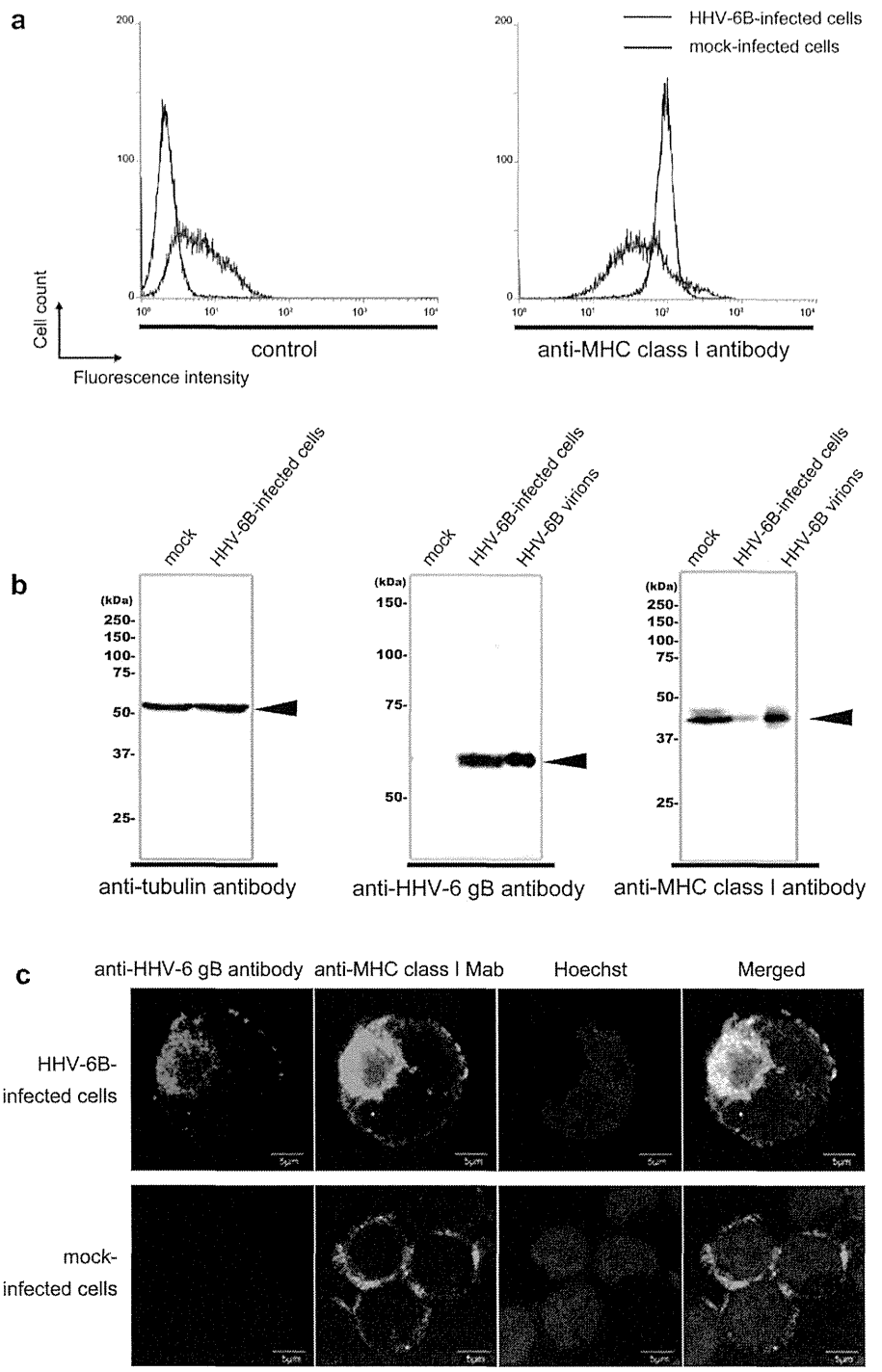

Fig. 2. Expression of MHC class I in HHV-6B-infected cells. (a) Expression of MHC class I on the surface of HHV-6B-infected cells is downregulated. HHV-6B-infected or mock-infected cells were harvested at 72 hr post-infection and fixed with 4% (w/v) paraformaldehyde. Fixed cells were stained with an anti-MHC class I antibody followed by staining with a secondary antibody prior to flow cytometric analysis. Control samples were incubated with the secondary antibody alone. Black histogram, mock-infected cells; blue histogram, HHV-6B- infected cells. (b) The total expression of MHC class I in HHV-6-infected cells was reduced. HHV-6B-infected or mock-infected cells were harvested at 72 hr post-infection and cell lysates prepared for western blotting. Purified HHV-6B virions were also used for western blotting. (c) MHC class I colocalizes with HHV-6B gB in intracellular compartments. HHV-6B-infected or mock-infected cells were harvested at 72 hr post-infection and fixed in cold acetone–methanol. Fixed cells were stained with antibodies against HHV-6 gB or MHC class I and with Hoechst33342. The stained cells were observed under a confocal microscope. The merged panels show the colocalized HHV-6 gB and MHC class I molecules. Single sections are shown. Scale bars: 5 micro meter.

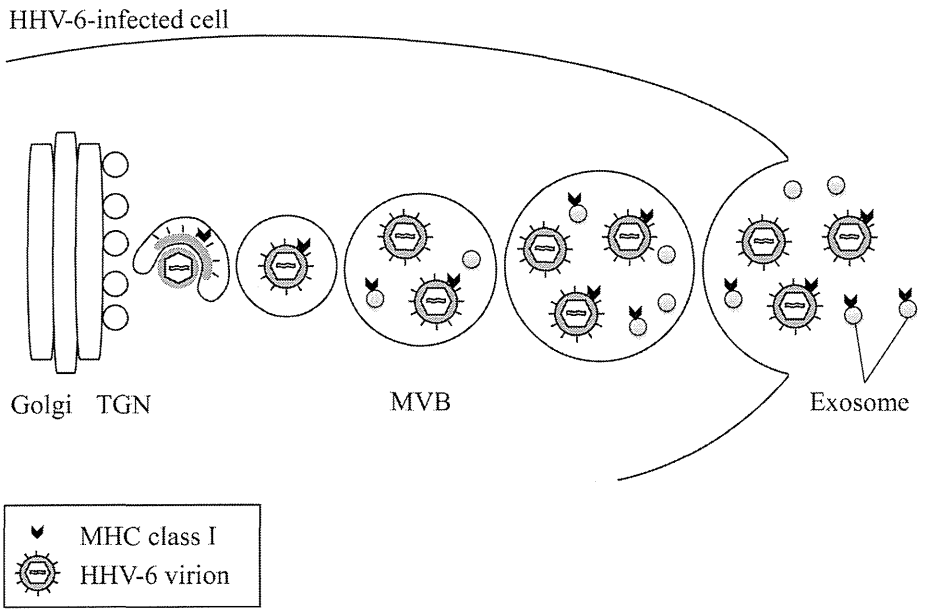

Fig. 3. Scematic representation of the fate of MHC class I molecules in HHV-6-infected cells. MHC class I molecules are transported to TGN- or post-TGN-derived vacuoles in HHV-6-infected cells and then incorporated into virions and intracellular small vesicles, which later become exosomes. Finally, MHC class I molecules are released from HHV-6-infected cells along with virions and exosomes.

within HHV-6-infected cells may show the combined characteristics of early and late endosomes. Recycling to early endosomes in HHV-6-infected cells may be modified or defective; therefore, several cellular proteins that use the same recycling system may be incorporated into virions and exosomes.

ACKNOWLEDGMENTS

We thank Dr. Kazushige Adachi (Minoh City Hospital) and Dr. Hideto Yamada (Department of Obstetrics and Gynecology, Kobe University Graduate School of Medicine) for providing the CBMCs. We also thank Ms. Eiko Moriishi (National Institute of Biomedical Innovation) for her technical support. This study was supported in part by a Grant-in-Aid for Scientific Research (B) and a Grant-in-Aid for Exploratory Research from the Japan Society for the Promotion of Science (JSPS).

DISCLOSURE

The authors declare that they have no competing interests.

REFERENCES

1. Roizmann B., Desrosiers R.C., Fleckenstein B., Lopez C., Minson A.C., Studdert M.J. (1992) The family Herpesviridae: an update. The Herpesvirus Study Group of the International Committee on Taxonomy of Viruses. *Arch Virol* **123**: 425–49.
2. Salahuddin S.Z., Ablashi D.V., Markham P.D., Josephs S.F., Sturzenegger S., Kaplan M., Halligan G., Biberfeld P., Wong-Staal F., Kramarsky B., Gallo R.C. (1986) Isolation of a new virus, HBLV, in patients with lymphoproliferative disorders. *Science* **234**: 596–601.
3. Aubin J.T., Collandre H., Candotti D., Ingrand D., Rouzioux C., Burgard M., Richard S., Huraux J.M., Agut H. (1991) Several groups among human herpesvirus 6 strains can be distinguished by Southern blotting and polymerase chain reaction. *J Clin Microbiol* **29**: 367–72.
4. Campadelli-Fiume G., Guerrini S., Liu X., Foa-Tomasi L. (1993) Monoclonal antibodies to glycoprotein B differentiate human herpesvirus 6 into two clusters, variants A and B. *J Gen Virol* **74**(Pt 10) 2257–62.
5. Wyatt L.S., Balachandran N., Frenkel N. (1990) Variations in the replication and antigenic properties of human herpesvirus 6 strains. *J Infect Dis* **162**: 852–7.
6. Yamanishi K., Okuno T., Shiraki K., Takahashi M., Kondo T., Asano Y., Kurata T. (1988) Identification of human herpesvirus-6 as a causal agent for exanthem subitum. *Lancet* **1**: 1065–7.
7. Okuno T., Takahashi K., Balachandra K., Shiraki K., Yamanishi K., Takahashi M., Baba K. (1989) Seroepidemiology of human herpesvirus 6 infection in normal children and adults. *J Clin Microbiol* **27**: 651–3.
8. Ahn K., Gruhler A., Galocha B., Jones T.R., Wiertz E.J., Ploegh H.L., Peterson P.A., Yang Y., Fruh K. (1997) The ER-luminal domain of the HCMV glycoprotein US6 inhibits peptide translocation by TAP. *Immunity* **6**: 613–21.
9. Hill A., Jugovic P., York I., Russ G., Bennink J., Yewdell J., Ploegh H., Johnson D. (1995) Herpes simplex virus turns off the TAP to evade host immunity. *Nature* **375**: 411–5.

10. Tomazin R., Van Schoot N.E., Goldsmith K., Jugovic P., Sempe P., Fruh K., Johnson D.C. (1998) Herpes simplex virus type 2 ICP47 inhibits human TAP but not mouse TAP. *J Virol* **72**: 2560–3.
11. Wills M.R., Ashiru O., Reeves M.B., Okecha G., Trowsdale J., Tomasec P., Wilkinson G.W., Sinclair J., Sissons J.G. (2005) Human cytomegalovirus encodes an MHC class I-like molecule (UL142) that functions to inhibit NK cell lysis. *J Immunol* **175**: 7457–65.
12. Jones T.R., Wiertz E.J., Sun L., Fish K.N., Nelson J.A., Ploegh H.L. (1996) Human cytomegalovirus US3 impairs transport and maturation of major histocompatibility complex class I heavy chains. *Proc Natl Acad Sci USA* **93**: 11,327–33.
13. Wiertz E.J., Jones T.R., Sun L., Bogyo M., Geuze H.J., Ploegh H.L. (1996) The human cytomegalovirus US11 gene product dislocates MHC class I heavy chains from the endoplasmic reticulum to the cytosol. *Cell* **84**: 769–79.
14. Ziegler H., Thale R., Lucin P., Muranyi W., Flohr T., Hengel H., Farrell H., Rawlinson W., Koszinowski U.H. (1997) A mouse cytomegalovirus glycoprotein retains MHC class I complexes in the ERGIC/cis-Golgi compartments. *Immunity* **6**: 57–66.
15. Coscoy L., Ganem D. (2000) Kaposi's sarcoma-associated herpesvirus encodes two proteins that block cell surface display of MHC class I chains by enhancing their endocytosis. *Proc Natl Acad Sci USA* **97**: 8051–6.
16. Hudson A.W., Howley P.M., Ploegh H.L. (2001) A human herpesvirus 7 glycoprotein, U21, diverts major histocompatibility complex class I molecules to lysosomes. *J Virol* **75**: 12347–58.
17. Ishido S., Wang C., Lee B.S., Cohen G.B., Jung J.U. (2000) Downregulation of major histocompatibility complex class I molecules by Kaposi's sarcoma-associated herpesvirus K3 and K5 proteins. *J Virol* **74**: 5300–9.
18. Reusch U., Muranyi W., Lucin P., Burgert H.G., Hengel H., Koszinowski U.H. (1999) A cytomegalovirus glycoprotein re-routes MHC class I complexes to lysosomes for degradation. *EMBO J* **18**: 1081–91.
19. Hirata Y., Kondo K., Yamanishi K. (2001) Human herpesvirus 6 downregulates major histocompatibility complex class I in dendritic cells. *J Med Virol* **65**: 576–83.
20. Glosson N.L., Hudson A.W. (2007) Human herpesvirus-6A and -6B encode viral immunoevasins that downregulate class I MHC molecules. *Virology* **365**: 125–35.
21. Mori Y., Yagi H., Shimamoto T., Isegawa Y., Sunagawa T., Inagi R., Kondo K., Tano Y., Yamanishi K. (1998) Analysis of human herpesvirus 6 U3 gene, which is a positional homolog of human cytomegalovirus UL 24 gene. *Virology* **249**: 129–39.
22. Mori Y., Akkapaiboon P., Yang X., Yamanishi K. (2003) The human herpesvirus 6 U100 gene product is the third component of the gH-gL glycoprotein complex on the viral envelope. *J Virol* **77**: 2452–8.
23. Mori Y., Koike M., Moriishi E., Kawabata A., Tang H., Oyaizu H., Uchiyama Y., Yamanishi K. (2008) Human herpesvirus-6 induces MVB formation, and virus egress occurs by an exosomal release pathway. *Traffic* **9**: 1728–42.
24. Okuno T., Shao H., Asada H., Shiraki K., Takahashi M., Yamanishi K. (1992) Analysis of human herpesvirus 6 glycoproteins recognized by monoclonal antibody OHV1. *J Gen Virol* **73**(Pt 2) 443–7.
25. Tang H., Kawabata A., Takemoto M., Yamanishi K., Mori Y. (2008) Human herpesvirus-6 infection induces the reorganization of membrane microdomains in target cells, which are required for virus entry. *Virology* **378**: 265–71.
26. Kawabata A., Tang H.M., Huang H.L., Yamanishi K., Mori Y. (2009) Human herpesvirus 6 envelope components enriched in lipid rafts: evidence for virion-associated lipid rafts. *Virology J* **6**: 127.
27. Yamada M., Mugnai G., Serada S., Yagi Y., Naka T., Sekiguchi K. (2013) Substrate-attached materials are enriched with tetraspanins and are analogous to the structures associated with rear-end retraction in migrating cells. *Cell Adh Migr* **7**: 304–14.
28. Akkapaiboon P., Mori Y., Sadaoka T., Yonemoto S., Yamanishi K. (2004) Intracellular processing of human herpesvirus 6 glycoproteins Q1 and Q2 into tetrameric complexes expressed on the viral envelope. *J Virol* **78**: 7969–83.
29. Mori Y., Akkapaiboon P., Yonemoto S., Koike M., Takemoto M., Sadaoka T., Sasamoto Y., Konishi S., Uchiyama Y., Yamanishi K. (2004) Discovery of a second form of tripartite complex containing gH-gL of human herpesvirus 6 and observations on CD46. *J Virol* **78**: 4609–16.
30. Raposo G., Nijman H.W., Stoorvogel W., Liejendekker R., Harding C.V., Melief C.J., Geuze H.J. (1996) B lymphocytes secrete antigen-presenting vesicles. *J Exp Med* **183**: 1161–72.
31. Elboim M., Grodzovski I., Djian E., Wolf D.G., Mandelboim O. (2013) HSV-2 specifically down regulates HLA-C expression to render HSV-2-infected DCs susceptible to NK cell killing. *PLoS Pathog* **9**: e1003226.
32. Kubota A., Kubota S., Farrell H.E., Davis-Poynter N., Takei F. (1999) Inhibition of NK cells by murine CMV-encoded class I MHC homologue m144. *Cell Immunol* **191**: 145–51.
33. Ma G., Feineis S., Osterrieder N., Van De Walle G.R. (2012) Identification and characterization of equine herpesvirus type 1 pUL56 and its role in virus-induced downregulation of major histocompatibility complex class I. *J Virol* **86**: 3554–63.
34. Neumann L., Kraas W., Uebel S., Jung G., Tampe R. (1997) The active domain of the herpes simplex virus protein IC P47: a potent inhibitor of the transporter associated with antigen processing. *J Mol Biol* **272**: 484–92.
35. Raafat N., Sadowski-Cron C., Mengus C., Heberer M., Spagnoli G.C., Zajac P. (2012) Preventing vaccinia virus class-I epitopes presentation by HSV-ICP47 enhances the immunogenicity of a TAP-independent cancer vaccine epitope. *Int J Cancer* **131**: E659–69.
36. Said A., Azab W., Damiani A., Osterrieder N. (2012) Equine herpesvirus type 4 UL56 and UL49.5 proteins downregulate cell surface major histocompatibility complex class I expression independently of each other. *J Virol* **86**: 8059–71.
37. Vasireddi M., Hilliard J. (2012) Herpes B virus, macacine herpesvirus 1, breaks simplex virus tradition via major histocompatibility complex class I expression in cells from human and macaque hosts. *J Virol* **86**(12) 503–11.

OPEN ACCESS Freely available online

PLOS | ONE

The Inhibition of N-Glycosylation of Glycoprotein 130 Molecule Abolishes STAT3 Activation by IL-6 Family Cytokines in Cultured Cardiac Myocytes

Reo Matsuo[9], Hirofumi Morihara[9], Tomomi Mohri, Shiho Murasawa, Kana Takewaki, Hiroyuki Nakayama, Makiko Maeda*, Yasushi Fujio*

Graduate School of Pharmaceutical Sciences, Osaka University, Suita City, Osaka, Japan

Abstract

Interleukin-6 (IL-6) family cytokines play important roles in cardioprotection against pathological stresses. IL-6 cytokines bind to their specific receptors and activate glycoprotein 130 (gp130), a common receptor, followed by further activation of STAT3 and extracellular signal-regulated kinase (ERK)1/2 through janus kinases (JAKs); however the importance of glycosylation of gp130 remains to be elucidated in cardiac myocytes. In this study, we examined the biological significance of gp130 glycosylation using tunicamycin (Tm), an inhibitor of enzyme involved in N-linked glycosylation. In cardiomyocytes, the treatment with Tm completely replaced the glycosylated form of gp130 with its unglycosylated one. Tm treatment inhibited leukemia inhibitory factor (LIF)-mediated activation of STAT3 and ERK1/2. Similarly, IL-11 failed to activate STAT3 and ERK1/2 in the presence of Tm. Interestingly, Tm inhibited the activation of JAKs 1 and 2, without influencing the expression of suppressor of cytokine signalings (SOCSs) and protein-tyrosine phosphatase 1B (PTP1B), which are endogenous inhibitors of JAKs. To exclude the possibility that Tm blocks LIF and IL-11 signals by inhibiting the glycosylation of their specific receptors, we investigated whether the stimulation with IL-6 plus soluble IL-6 receptor (sIL-6R) could transduce their signals in Tm-treated cardiomyocytes and found that this stimulation was unable to activate the downstream signals. Collectively, these findings indicate that glycosylation of gp130 is essential for signal transduction of IL-6 family cytokines in cardiomyocytes.

Citation: Matsuo R, Morihara H, Mohri T, Murasawa S, Takewaki K, et al. (2014) The Inhibition of N-Glycosylation of Glycoprotein 130 Molecule Abolishes STAT3 Activation by IL-6 Family Cytokines in Cultured Cardiac Myocytes. PLoS ONE 9(10): e111097. doi:10.1371/journal.pone.0111097

Editor: Shree Ram Singh, National Cancer Institute, United States of America

Received April 9, 2014; **Accepted** September 29, 2014; **Published** October 23, 2014

Data Availability: The authors confirm that all data underlying the findings are fully available without restriction. All relevant data are within the paper.

Funding: This study was supported by a grant-in-aid for scientific research from the Japan society for the promotion of science; YF, HN, MM. This study was supported by MEXT/JSPS KAKENHI Grant Numbers 23390057, 26293054, 25860061 and 22590160. The funders had no role in study design, data collection and analysis, decision to publish, or preparation of the manuscript.

Competing Interests: The authors have declared that no competing interests exist.

* Email: makikom@phs.osaka-u.ac.jp (MM); fujio@phs.osaka-u.ac.jp (YF)

[9] These authors contributed equally to this work.

Introduction

Accumulating evidence has demonstrated that interleukin-6 (IL-6) family cytokines play important roles in the maintenance of cardiac homeostasis [1]. Among IL-6 family cytokines, leukemia inhibitory factor (LIF), cardiotrophin-1 (CT-1), and IL-11, but not IL-6, have been reported to transduce their signals, such as signal transducers and activator of transcription (STAT)3 and extracellular signal-regulated kinase (ERK) 1/2 in cardiac myocytes [2,3]. These cytokines bind their specific receptor α subunits that are expressed in cardiac myocytes and activate their common receptor subunit, glycoprotein 130 (gp130) [4]. Since the activation of gp130 is essential for the signal transduction of IL-6 family cytokines, the structure of gp130 molecule has been intensively investigated. As a result, structural biological studies have proposed the glycosylation sites on gp130 molecule [5]; however, the biological significance of the glycosylation of gp130 remains to be fully elucidated in cardiac myocytes.

Tunicamycin (Tm), an inhibitor of N-acetylglucosamine phosphotransferase, is widely used as an inducer of endoplasmic reticulum (ER) stress [6]. Tm treatment induces ER stress by inhibiting N-glycosylation of cell surface and secreted glycoproteins in the ER and Golgi. Interestingly, it was recently demonstrated that ER stress causes leptin resistance [7,8]. Under the condition of ER stress, protein-tyrosine phosphatase 1B (PTP1B) plays important roles in the suppression of leptin signaling by inhibiting janus kinase (JAK) 2 activity and leptin fails to activate JAK2/STAT3 pathway in the presence of Tm. Though leptin receptor structurally resembles gp130, utilizing JAK/STAT pathway [9], the effects of Tm on gp130 signaling in cardiomyocytes remain to be fully addressed.

In this study, we examined the effects of Tm on the glycosylation of gp130 and its downstream signals in cardiac myocytes. Tm treatment completely replaced glycosylated gp130 with its unglycosylated form and inhibited STAT3 and ERK1/2 activation by IL-6 family cytokines in cultured cardiac myocytes. Based on these findings, we concluded that the N-glycosylation of gp130 is essential for the signal transduction through gp130.

Table 1. The primers used in this study.

Genes	Direction	Sequence
CHOP	Forward	5′-GCACCTCCCAGAGCCCTCACTCTCC-3′
	reverse	5′-GTCTACTCCAAGCCTTCCCCCTGCG-3′
Grp78	forward	5′-GAAGGGGAGCAGAAAGCCCAT-3′
	reverse	5′-GCTTTGGTGAGGTTTGATCCGC-3′
SOCS1	forward	5′-CCGCTCCCACTCTGATTACC-3′
	reverse	5′-CGAAGCCATCTTCACGCTGA-3′
SOCS3	forward	5′-CGACGGAACCTTCCTTTGAGG-3′
	reverse	5′-TAGCCACGTTGGAGGAGAGAG-3′
PTP1B	forward	5′-TGCACAGCATGAGCAGTATG-3′
	reverse	5′-TGTGCCTTTTGTTCCTCCTC-3′
GAPDH	forward	5′-CATCACCATCTTCCAGGAGCG-3′
	reverse	5′-GAGGGGCCATCCACAGTCTTC-3′

doi:10.1371/journal.pone.0111097.t001

Materials and Methods

Ethics statement

The experiments using animals were approved by the Institutional Animal Care and Use Committee of Graduate School of Pharmaceutical Sciences, Osaka University (Permit Number; DOUYAKU19-32-6). The care of all animals was performed in compliance with the Osaka University animal care guidelines.

Cell culture

Neonatal rat cardiomyocytes were cultured as described previously [10]. In brief, after the rats were anesthetized with isoflurane, hearts were excised, minced and digested with solution containing 0.1% collagenase type IV and 0.1% trypsin to obtain a single-cell suspension. After preplating the cells on culture dish for 60 minutes, floating cells were used as cardiomyocytes. Isolated cardiomyocytes were cultured in Dulbecco's Modified Eagles Medium (D-MEM); high glucose with L-Glutamine and sodium bicarbonate (Sigma-Aldrich) supplemented with 10% fetal bovine serum and bromodeoxyuridine (0.1 μg/mL).

To analyze the effects of Tm, cultured cardiomyocytes were treated with the indicated concentrations of Tm for the indicated hours. Cells were washed with serum free medium and used for experiments. Cells were stimulated with LIF (300 units/mL), IL-11 (20 ng/mL) or IL-6 (20 ng/mL) plus soluble IL-6 receptor (sIL-6R) (100 ng/mL) for 15 minutes.

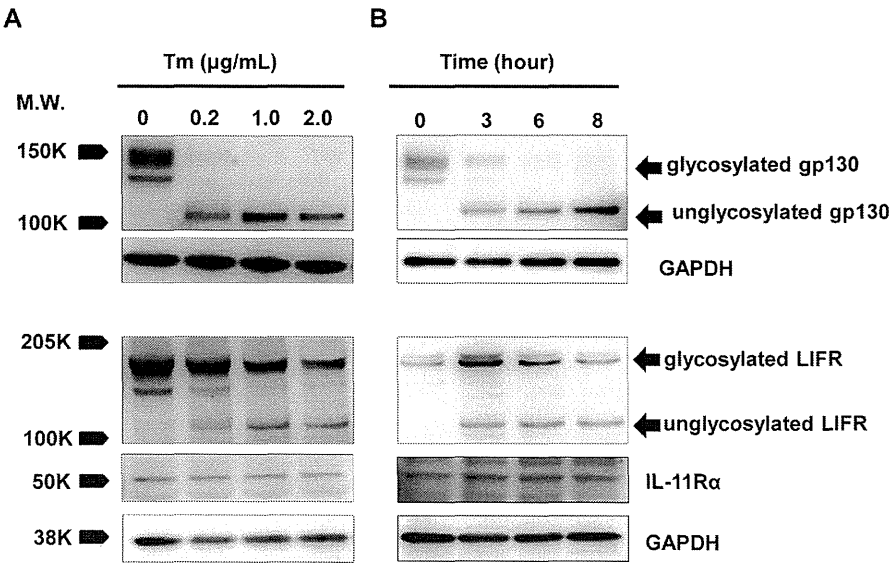

Figure 1. Tunicamycin inhibits the glycosylation of gp130 completely, but does those of LIFR and IL-11Rα partially. Neonatal rat cardiomyocytes were treated with the indicated concentrations of Tm for 8 hrs (A), or with 2 μg/mL of Tm for the indicated times (B), respectively. After each treatment, cell lysates were prepared and immunoblotted with anti-gp130, LIFR or IL-11Rα antibody, respectively. More than three independent experiments were performed with similar results and representative images were shown.
doi:10.1371/journal.pone.0111097.g001